

AD-A042 347

MISSISSIPPI UNIV UNIVERSITY
DYNAMIC ANALYSIS OF A LOADED CONICAL ANTENNA OVER A GROUND PLAN--ETC(U)
JUL 77 D R WILTON

F/G 9/5
AF-AFOSR-2825-75

UNCLASSIFIED

AFWL-TR-77-55

NL

| OF |
AD
A042347



END
DATE
FILMED
8-77
DDC

AFWL-TR-77-55

AFWL-TR-
77-55

2

ADA 042347

DYNAMIC ANALYSIS OF A LOADED CONICAL ANTENNA OVER A GROUND PLANE

University of Mississippi
University, MS 38677

July 1977

Final Report



Approved for public release; distribution unlimited

AU NO. 1
DDC FILE COPY

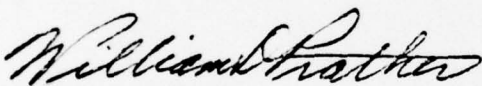
AIR FORCE WEAPONS LABORATORY
Air Force Systems Command
Kirtland Air Force Base, NM 87117

This final report was prepared by the University of Mississippi, University, Mississippi, under AFOSR Grants 75-2825 and 75-2832, Job Order 12090505, with the Air Force Weapons Laboratory, Kirtland Air Force Base, New Mexico. Mr William D Prather (ELP) was the Laboratory Project Officer-in-Charge.

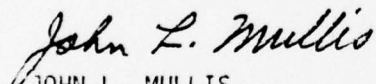
When US Government drawings, specifications, or other data are used for any purpose other than a definitely related Government procurement operation, the Government thereby incurs no responsibility nor any obligation whatsoever, and the fact that the Government may have formulated, furnished, or in any way supplied the said drawings, specifications, or other data is not to be regarded by implication or otherwise as in any manner licensing the holder or any other person or corporation or conveying any rights or permission to manufacture, use or sell any patented invention that may in any way be related thereto.

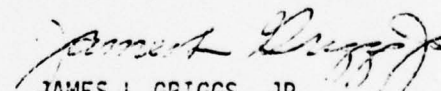
This report has been reviewed by the Office of Information (OI) and is releasable to the National Technical Information Service (NTIS). At NTIS, it will be will be available to the general public, including foreign nations.

This technical report has been reviewed and is approved for publication.


WILLIAM D PRATHER
Project Officer

FOR THE COMMANDER


JOHN L. MULLIS
Acting Chief
Phenomenology and Technology Branch


JAMES L GRIGGS, JR
Colonel, USAF
Chief, Electronics Division

UNCLASSIFIED

SECURITY CLASSIFICATION OF THIS PAGE (When Data Entered)

REPORT DOCUMENTATION PAGE		READ INSTRUCTIONS BEFORE COMPLETING FORM
1. REPORT NUMBER AFWL-TR-77-55	2. GOVT ACCESSION NO.	3. RECIPIENT'S CATALOG NUMBER
4. TITLE (and Subtitle) DYNAMIC ANALYSIS OF A LOADED CONICAL ANTENNA OVER A GROUND PLANE	5. TYPE OF REPORT & PERIOD COVERED Final Report	
7. AUTHOR(s) Donald R. Wilton	6. PERFORMING ORG. REPORT NUMBER	
9. PERFORMING ORGANIZATION NAME AND ADDRESS University of Mississippi University, Mississippi 38677	8. CONTRACT OR GRANT NUMBER(s) AFOSR Grant No. 75-2825-75 AFOSR Grant No. 75-2832-75	
11. CONTROLLING OFFICE NAME AND ADDRESS Air Force Weapons Laboratory (ELP) Kirtland Air Force Base, NM 87117	10. PROGRAM ELEMENT, PROJECT, TASK AREA & WORK UNIT NUMBERS 61102F & 64747F 12090505	
14. MONITORING AGENCY NAME & ADDRESS (if different from Controlling Office)	12. REPORT DATE July 1977	
	13. NUMBER OF PAGES 86	
	15. SECURITY CLASS. (of this report) UNCLASSIFIED	
	15a. DECLASSIFICATION/DOWNGRADING SCHEDULE	
16. DISTRIBUTION STATEMENT (of this Report) Approved for public release; distribution unlimited		
17. DISTRIBUTION STATEMENT (of the abstract entered in Block 20, if different from Report)		
18. SUPPLEMENTARY NOTES This research was jointly sponsored by the AFWL and the Air Force Office of Scientific Research		
19. KEY WORDS (Continue on reverse side if necessary and identify by block number) Electricity and magnetism Biconical Electromagnetic fields and waves Loaded Antennas Conical		
20. ABSTRACT (Continue on reverse side if necessary and identify by block number) Three integral equations are derived and formulated for numerical solution for the currents induced on a resistively loaded conical antenna over a ground plane. The first integral equation is a relatively simple one for a cone without a top-cap. The second and third integral equations are applicable to a cone with or without a topcap, but the latter equation is relatively cumbersome, involving complicated kernels with various singularities. A computer code has been developed for each of the three methods. Numerical data for current distributions (Con't)		

234450

Jmc

UNCLASSIFIED

SECURITY CLASSIFICATION OF THIS PAGE (When Data Entered)

20. Abstract. (Con't)

input impedances and radiation patterns are presented for resistively loaded and unloaded structures, both with and without topcap. ↗

ADMISSION TO

NTIS	White Section	<input checked="" type="checkbox"/>
DOC	Buff Section	<input type="checkbox"/>
UNANNOUNCED		<input type="checkbox"/>

JUSTIFICATION

BY

DISTRIBUTION/AVAILABILITY CODES

Dist.	AVAIL. and/or	SPECIAL
A		

CONTENTS

SECTION		PAGE
I	INTRODUCTION	1
II	FORMULATION OF AN INTEGRAL EQUATION FOR A BICONE WITHOUT ENDCAPS	2
III	APPLICATION OF METHOD OF MOMENTS TO A BICONE WITHOUT ENDCAPS	9
IV	FORMULATION AND NUMERICAL SOLUTION OF AN INTEGRAL EQUATION FOR A BICONE WITH ENDCAPS	19
V	NUMERICAL RESULTS AND CONCLUSIONS	34
	REFERENCES	61
APP A	CALCULATION OF RADIATED FIELDS	63
APP B	AN ALTERNATE INTEGRAL EQUATION FOR A CONE WITH TOPCAP	66

ILLUSTRATIONS

FIGURE		PAGE
1	Geometry of Cone Over a Ground Plane	3
2	Testing Functions for the Cone	10
3	Pulse Expansion Functions for the Current on the Cone	15
4	Geometry of Cone with Endcap	21
5	Pulse Expansion and Testing Functions	25
6	Pulse Expansions for the Charge on the Cone	28
7	Current on Unloaded Cone with Topcap, $L=54.05m$, $\theta_0 = 42.26^\circ$, $V_0 = 1$ Volt, $f = 825$ KHz	37
8	Current on unloaded Cone without Topcap, $L = 54.05m$, $\theta_0 = 42.26^\circ$, $V_0 = 1$ Volt, $f = 825$ KHz	38
9	Current on Loaded Cone with Topcap, $L = 54.05m$, $\theta_0 = 42.26^\circ$, $V_0 = 1$ Volt, $f = 825$ KHz	39
10	Current on Loaded Cone without Topcap, $L = 54.05m$, $\theta_0 = 42.26^\circ$, $V_0 = 1$ Volt, $f = 825$ MHz	40
11	Current on Unloaded Cone with Topcap, $L = 54.05m$, $\theta_0 = 42.26^\circ$, $V_0 = 1$ Volt, $f = 1.375$ MHz	41
12	Current on Unloaded Cone without Topcap, $L = 54.05m$, $\theta_0 = 42.26^\circ$, $V_0 = 1$ Volt, $f = 1.375$ MHz	42
13	Current on Loaded Cone with Topcap, $L = 54.05m$, $\theta_0 = 42.26^\circ$, $V_0 = 1$ Volt, $f = 1.375$ MHz	43
14	Current on Loaded Cone without Topcap, $L=54.05m$, $\theta_0 = 42.26^\circ$, $V_0 = 1$ Volt, $f = 1.375$ MHz	44
15	Input Impedance of Unloaded Cone with Topcap, $L = 54.05m$, $\theta_0 = 42.26^\circ$. Encircled Values of Imaginary Part are Positive	45
16	Input Impedance of Unloaded Cone without Topcap, $L = 54.05m$, $\theta_0 = 42.26^\circ$. Encircled Values of Imaginary Part are Positive	46

FIGURE		PAGE
17	Input Impedance of Loaded Cone with Topcap L = 54.05m, $\theta_0 = 42.26^\circ$, Imaginary Values are Negative	47
18	Input Impedance of Loaded Cone without Topcap, L = 54.05m, $\theta_0 = 42.26^\circ$. Imaginary Values are Negative	48
19	E_θ radiation pattern for loaded cone with Topcap, L = 54.05m, $\theta_0 = 42.26^\circ$, $V_0 = 1$ Volt, f = 550 KHz, r = 100m	50
20	H_ϕ Radiation Pattern for Loaded Cone with Topcap, L = 54.05m, $\theta_0 = 42.26^\circ$, $V_0 =$ 1 Volt, f = 550 KHz, r = 100 m	51
21	E_r Radiation Pattern for Loaded Cone with Topcap, L = 54.05m, $\theta_0 = 42.26^\circ$, $V_0 =$ 1 Volt, f = 550 KHz, r = 100m	52
22	E_θ Radiation Pattern for Loaded Cone with Topcap, L = 54.05m, $\theta_0 = 42.26^\circ$, $V_0 =$ 1 Volt, f = 550 KHz, r = 10 m	53
23	H_ϕ Radiation Pattern for Loaded Cone with Topcap, L = 54.05m, $\theta_0 = 42.26^\circ$, $V_0 =$ 1 Volt, f = 550 KHz, r = 10 m	54
24	E_r Radiation Pattern for Loaded Cone with Topcap, L = 54.05m, $\theta_0 = 42.26^\circ$, $V_0 =$ 1 Volt, f = 550 KHz, r = 10 m	55
25	E_θ Radiation Pattern for Unloaded Cone with Topcap, L = 54.05m, $\theta_0 = 42.26^\circ$, $V_0 = 1$ Volt, f = 550 KHz, r = 10 m	56
26	H_ϕ Radiation Pattern for Unloaded Cone with Topcap, L = 54.05m, $\theta_0 = 42.26^\circ$, $V_0 = 1$ Volt, f = 550 KHz, r = 10 m	57
27	E_r Radiation Pattern for Unloaded Cone with Topcap, L = 54.05m, $\theta = 42.26^\circ$, $V_0 = 1$ Volt, f = 550 KHz, r = 10 m	58

SECTION I
INTRODUCTION

In a companion report [1], the static analysis of a conical antenna over a ground plane is presented. In this report, the analysis is extended to treat the time-harmonic case and to incorporate a model of the resistive loading of the structure. The resistive loading is intended to reduce the effect of diffraction from the cone edge at the higher frequencies.

If the cone has no topcap, the analysis may be considerably simplified and a simple integral equation for this situation is derived in Section II and implementation of a moment method solution is considered in Section III. In Section IV, an integral equation for the cone with a topcap is derived. Presented in Section V are numerical results in the frequency domain for currents on a loaded conical antenna both with and without a topcap. In Appendix A expressions are derived for the computation of fields from the currents and Appendix B gives the derivation of an alternate integral equation from that derived in Section IV.

PRECEDING PAGE BLANK NOT FILMED

SECTION II
FORMULATION OF AN INTEGRAL EQUATION FOR
A BICONE WITHOUT ENDCAPS

For the symmetrically driven biconical structure of Figure 1, the current on both the cone and its image are radially directed and have no circumferential (ϕ) variation. Hence the magnetic field tangent to the cone is ϕ -directed and the boundary conditions can be satisfied by fields which are transverse magnetic (TM) to r . Thus, the fields may be completely determined by a radially-directed vector potential $\bar{A} = A_r \hat{r}$ [2]. In an eigenfunction solution to such problems, the fields are determined in the bicone region from a vector potential A_r which comes from a homogeneous solution of the wave equation. In order to derive an integral equation, however, A_r must be expressed in terms of the current on the bicone. In particular, a free space Green's function is to be found for the vector potential A_r due to a unit radially-directed current element. A superposition integral then expresses the total vector potential due to currents on the cone.

Beginning with the assumption that the magnetic field is determined from $\bar{A} = A_r \hat{r}$,

$$\bar{H} = \frac{1}{\mu} \nabla \times \bar{A}$$

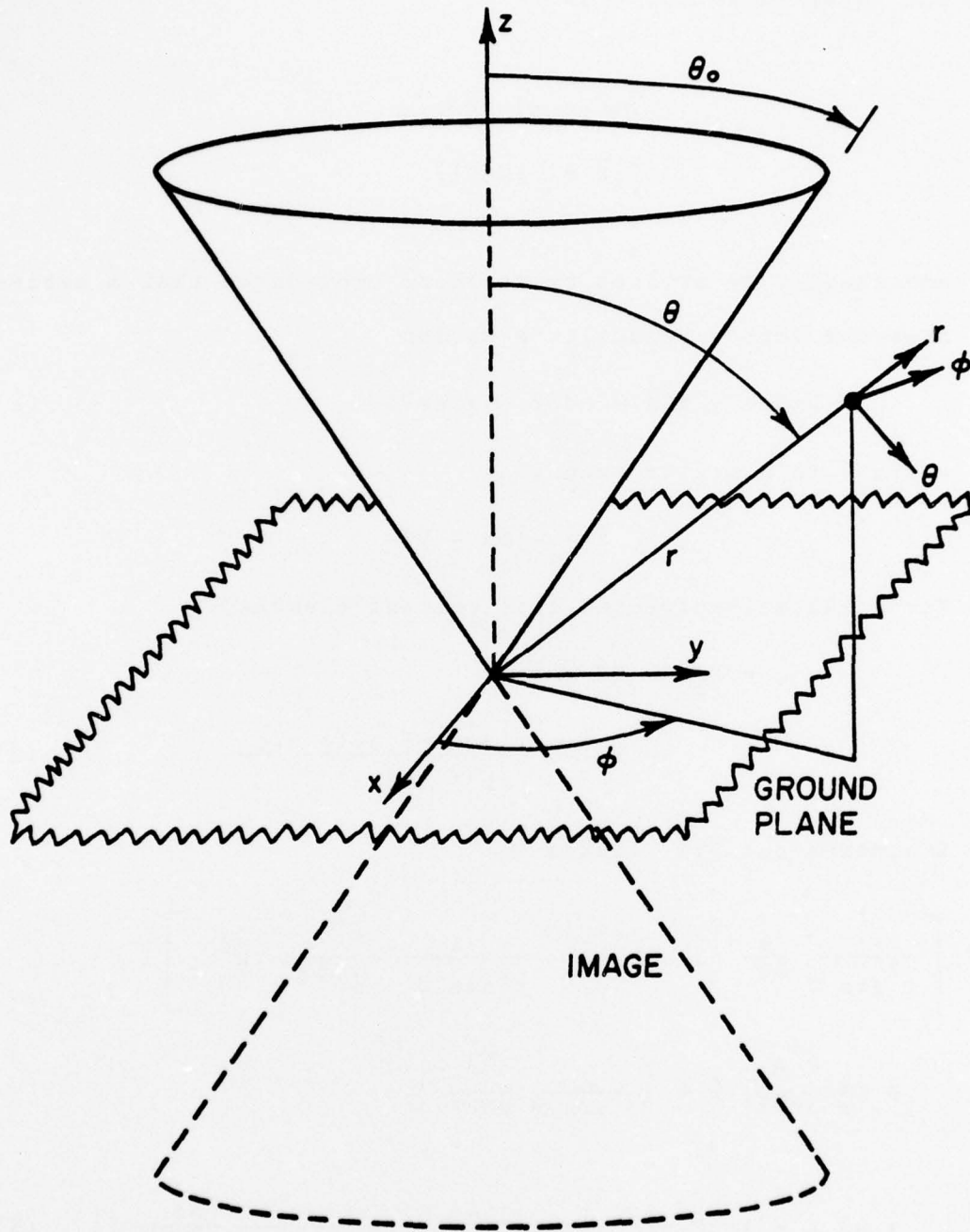


Figure 1. Geometry of cone over a ground plane.

and using Maxwell's equations,

$$\nabla \times \bar{E} = -j\omega\mu\bar{H}$$

$$\nabla \times \bar{H} = j\omega\epsilon\bar{E} + \bar{J}$$

one readily determines by standard procedures that \bar{A} satisfies the vector Helmholtz equation

$$\nabla \times \nabla \times \bar{A} - k^2 \bar{A} = \mu \bar{J}_r \hat{r} - j\omega\mu\epsilon \nabla \phi \quad (1)$$

where ϕ is a scalar such that

$$\bar{E} = -j\omega\bar{A} - \nabla\phi$$

For a radially-directed unit current element,

$$\begin{aligned} \bar{J} &= J_r \hat{r} = \hat{r} \delta(\bar{r} - \bar{r}') \\ &= \hat{r} \frac{\delta(r-r')\delta(\theta-\theta')\delta(\phi-\phi')}{r'^2 \sin \theta'} \end{aligned} \quad (2)$$

Expanding out (1) yields

$$\begin{aligned} &\left[\frac{-1}{r^2 \sin \theta} \frac{\partial}{\partial \theta} \left(\sin \theta \frac{\partial A_r}{\partial \theta} \right) - \frac{1}{r^2 \sin^2 \theta} \frac{\partial^2 A_r}{\partial \phi^2} - k^2 A_r \right] \hat{r} \\ &+ \left(\frac{1}{r} \frac{\partial^2 A_r}{\partial r \partial \theta} \right) \hat{\theta} + \left(\frac{1}{r \sin \theta} \frac{\partial^2 A_r}{\partial \phi \partial r} \right) \hat{\phi} \\ &= \mu J_r \hat{r} - j\omega\mu\epsilon \left(\frac{\partial \phi}{\partial r} \hat{r} + \frac{1}{r} \frac{\partial \phi}{\partial \theta} \hat{\theta} + \frac{1}{r \sin \theta} \frac{\partial \phi}{\partial \phi} \hat{\phi} \right) \end{aligned} \quad (3)$$

from which it is seen that

$$\frac{\partial^2 A_r}{\partial r \partial \theta} = -j\omega\mu\epsilon \frac{\partial \phi}{\partial \theta}$$

$$\frac{\partial^2 A_r}{\partial \phi \partial r} = -j\omega\mu\epsilon \frac{\partial \phi}{\partial \phi} \quad (4)$$

These conditions are automatically satisfied by the gauge choice

$$\phi = -\frac{1}{j\omega\mu\epsilon} \frac{\partial A_r}{\partial r} \quad (5)$$

Substituting (2) and (5) into (3) leaves the one scalar component equality

$$\begin{aligned} \frac{\partial^2 A_r}{\partial r^2} + \frac{1}{r^2 \sin^2 \theta} \frac{\partial}{\partial \theta} \left(\sin^2 \theta \frac{\partial A_r}{\partial \theta} \right) + \frac{1}{r^2 \sin^2 \theta} \frac{\partial^2 A_r}{\partial \phi^2} \\ + k^2 A_r = -\mu \delta(\vec{r} - \vec{r}') \end{aligned} \quad (6)$$

which can be rewritten in the more convenient form,

$$(\nabla^2 + k^2) \left(\frac{A_r}{r} \right) = \frac{-\mu \delta(\vec{r} - \vec{r}')}{r'} \quad (7)$$

To obtain (7), one notes that

$$\frac{\delta(\vec{r} - \vec{r}')}{r} = \frac{\delta(\vec{r} - \vec{r}')}{r'}$$

A solution of (7) which satisfies the radiation condition for a $\exp(j\omega t)$ time convention may be written by inspection of (7) as

$$A_r = \frac{\mu r}{4\pi r'} \frac{e^{-jk|\bar{r}-\bar{r}'|}}{|\bar{r}-\bar{r}'|} \quad (8)$$

and the general solution to (3) for a distributed set of currents is obtained by superposition:

$$A_r = \frac{\mu}{4\pi} \int_V J_r(\bar{r}') \frac{r e^{-jk|\bar{r}-\bar{r}'|}}{r' |\bar{r}-\bar{r}'|} dV' \quad (9)$$

This form of the vector potential has also been used by others [3]. For the symmetrically-excited cone and its image,

$$J_r(\bar{r}') = \frac{J_{sr}(\bar{r}')}{r'} \left[\delta(\theta' - \theta_0) - \delta(\theta' - \pi + \theta_0) \right] \quad (10)$$

where J_{sr} is the bicone surface current density. Substituting (10) into (9) gives the desired equation for the vector potential:

$$A_r = \frac{\mu r \sin \theta_0}{4\pi} \int_0^{2\pi} \int_0^L J_{sr}(r') \left(\frac{e^{-jkR^+}}{R^+} - \frac{e^{-jkR^-}}{R^-} \right) dr' d\phi' \quad (11)$$

where

$$R^\pm = \sqrt{r^2 + r'^2 - 2rr'[\sin \theta \sin \theta_0 \cos(\phi - \phi') \pm \cos \theta \cos \theta_0]}$$

The plus superscript denotes source points on the upper bicone surface while the negative sign denotes source points on the image surface.

It is convenient to introduce the total axial current

$$I(r') = 2\pi r' \sin \theta_0 J_{sr}(r') \quad (12)$$

so that (11) becomes

$$A_r = \frac{\mu r}{8\pi^2} \int_0^{2\pi} \int_0^L \frac{I(r')}{r'} \left(\frac{e^{-jkR^+}}{R^+} - \frac{e^{-jkR^-}}{R^-} \right) dr' d\phi' \quad (13)$$

The radial component of electric field is now given by

$$E_r = \frac{1}{j\omega\mu\epsilon} \left(\frac{\partial^2}{\partial r^2} + k^2 \right) A_r \quad (14)$$

The simplicity of (13) and (14) compared to the usual vector potential representations should be emphasized at this point. One notes that in the usual representation, two vector potential components, A_r and A_θ , would be present. Furthermore, the integrands of the potential integrals would contain somewhat complicated dependences on angles between observation and source points which arise from projecting the source vector onto the potential component vector for each source and observation point. Finally, the expression for the radially-directed electric field would be complicated and difficult to handle numerically compared to the approach to be followed here. These complications indeed will appear in the formulation which includes a topcap on the bicone structure (Appendix B).

An integral equation for the current is obtained by applying the boundary condition that the radial electric field must equal the impedance loading times the total current density, i.e.,

$$E_r = Z_s(r)I(r)$$

Since all currents and fields are ϕ -independent, it suffices to take all observation points along the intersection of the plane $\phi=0$ and the conical surface. Hence, we obtain finally

$$\frac{1}{j\omega\mu\epsilon} \left(\frac{d^2}{dr^2} + k^2 \right) A_r - Z_s(r)I(r) = 0, \quad 0 < r \leq \ell, \quad \theta = \theta_0, \phi = 0 \quad (15)$$

Equation (15) is an integro-differential equation for the induced current on the bicone. As it stands, (15) does not appear to contain a driving term due to the applied voltage at the bicone terminals. In the next section, however, this term appears as a "boundary" condition on dA_r/dr at $r=0$. One also notes in (15) that discrete or lumped loading may be introduced by allowing $Z_s(r)$ to be represented by appropriate δ -functions,

$$Z_s(r) = \sum_{n=1}^{N_L} Z_{Ln} \delta(r-r_{Ln})$$

for N_L loads where Z_{Ln} is the impedance of the n^{th} load located at $r=r_{Ln}$.

SECTION III
 APPLICATION OF METHOD OF MOMENTS TO A
 BICONE WITHOUT ENDCAPS

The usual procedure in applying the method of moments [4] is to first represent the unknown current as a linear combination of an appropriate set of basis functions and then "test" the resulting integral equation with a series of testing functions. Here it is convenient to reverse this order and to first test the equation before expanding the current. A set of testing functions which offer a number of advantages in a numerical procedure are the piecewise sinusoidal testing functions:

$$w_1(r) = \begin{cases} \frac{\sin k(\Delta r - r)}{\sin k\Delta r} & , 0 \leq r \leq \Delta r \\ 0 & , \Delta r \leq r \leq L \end{cases}$$

$$w_m(r) = \begin{cases} \frac{\sin k(\Delta r - |r - r_m|)}{\sin k\Delta r} & , r_{m-1} \leq r \leq r_{m+1} \\ 0 & , |r - r_m| > \Delta r \end{cases}$$

$m = 2, 3, \dots, M \quad (16)$

where $\Delta r = L/M$, $r_m = (m-1)\Delta r$, $m=1, 2, \dots, M$.

These testing functions are shown in Figure 2. An inner product is next defined as

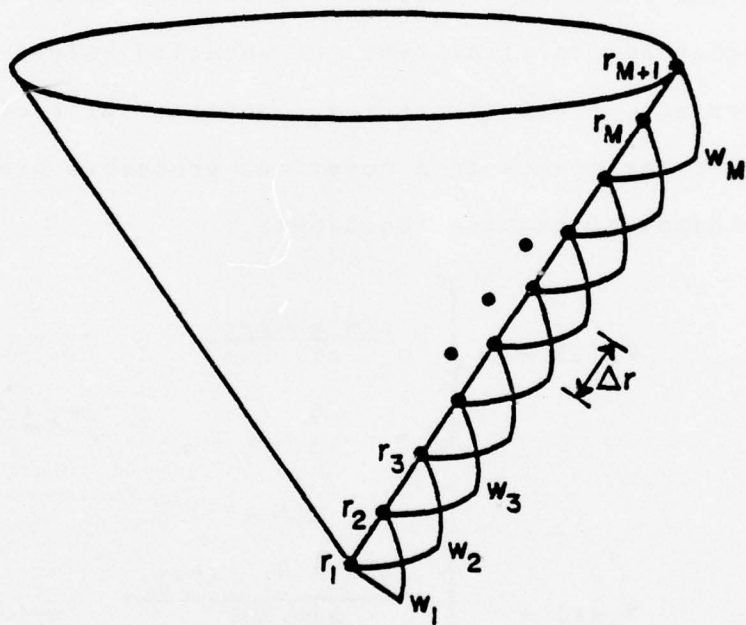


Figure 2. Testing functions for the cone.

$$\langle f(r), g(r) \rangle = \int_0^L f(r)g(r)dr \quad (17)$$

and (15) is successively tested with each of the w_m ,
 $m=1,2,\dots,M$:

$$\frac{1}{j\omega\mu\epsilon} \left\langle \left(\frac{d^2}{dr^2} + k^2 \right) A_r, w_m \right\rangle - \left\langle Z_s(r)I(r), w_m \right\rangle = 0, \quad m=1,2,\dots,M \quad (18)$$

Taking, for the moment, $m=1$ and integrating the first term by parts twice results in

$$\left\langle \left(\frac{d^2}{dr^2} + k^2 \right) A_r, w_1 \right\rangle = - \left. \frac{dA_r}{dr} \right|_{r=0} + \frac{k}{\sin k\Delta r} A_r(r_2) - \frac{k \cos k\Delta r}{\sin k\Delta r} A_r(r_2)$$

where $A_r(r_m) = A_r \Big|_{r=r_m}$. Note that although

$$A_r \Big|_{\theta=\pi/2} = 0, \quad (19)$$

$A_r(r_1)$ is not zero along the bicone. In fact, one notes that

$$E_\theta = \frac{1}{j\omega\mu\epsilon r} \frac{\partial^2 A_r}{\partial r \partial \theta}$$

and that the bicone voltage at $r=0$ is just

$$\begin{aligned}
V_0 &= \int_{\theta_0}^{\pi/2} E_{\theta} r d\theta \Big|_{r=0} \\
&= \frac{1}{j\omega\mu\epsilon} \int_{\theta_0}^{\pi/2} \frac{\partial^2 A_r}{\partial r \partial \theta} d\theta \Big|_{r=0} = - \frac{1}{j\omega\mu\epsilon} \frac{\partial A_r(r_1)}{\partial r}
\end{aligned}$$

where, using (19), one sees that $\partial A_r / \partial r = 0$ at $\theta = \pi/2$.

Thus for $m=1$, (18) becomes

$$\begin{aligned}
\frac{k}{j\omega\mu\epsilon \sin k\Delta r} \left[-\cos k\Delta r A_r(r_1) + A_r(r_2) \right] \\
- \left\langle Z_s(r) I(r), w_1 \right\rangle = -V_0 \quad (20)
\end{aligned}$$

For $m=2,3,4,\dots,M$, integration by parts twice in (18) results in

$$\begin{aligned}
\frac{k}{j\omega\mu\epsilon \sin k\Delta r} \left[A_r(r_{m+1}) - 2 \cos k\Delta r A_r(r_m) + A_r(r_{m-1}) \right] \\
- \left\langle Z_s(r) I(r), w_m \right\rangle = 0
\end{aligned}$$

$$m = 2, 3, \dots, M \quad (21)$$

Note that the choice of testing functions has resulted in removing all the derivative operations from the operator equations. This is the principal advantage of the testing functions chosen.

A matrix equation now results if the current is expanded in an appropriate set of basis functions. A convenient set is the pulse functions defined by

$$p_1(r) = \begin{cases} 1, & 0 \leq r \leq \Delta r/2 \\ 0, & \Delta r/2 \leq r \leq L \end{cases}$$

$$p_n(r) = \begin{cases} 1, & |r-r_n| \leq \Delta r/2 \\ 0, & |r-r_n| > \Delta r/2 \end{cases}$$

$$n = 2, 3, \dots, M$$

(see Figure 3) and the resulting current expansion is

$$I(r) \approx \sum_{n=1}^M I_n p_n(r) \quad (22)$$

Note that the current at the bicone edge $r=L$ is automatically zero by our choice of basis functions (Figure 3).

When (22) is substituted into (20) and (21), there results the system of linear equations

$$I_1 \left\{ \frac{k}{j\omega\mu\epsilon \sin k\Delta r} \left[-\cos k\Delta r \Psi(r_1; r_1, r_{1+}) + \Psi(r_2; r_2, r_{1+}) \right] - \left\langle Z_s(r) p_1(r), w_1 \right\rangle \right\} +$$

$$\begin{aligned}
& + \sum_{n=2}^M I_n \left\{ \frac{k}{j\omega\mu\epsilon \sin k\Delta r} \left[-\cos k\Delta r \Psi(r_1; r_{n-}, r_{n+}) + \Psi(r_2; r_{n-}, r_{n+}) \right] \right. \\
& \qquad \qquad \qquad \left. - \left\langle Z_s(r) p_n(r), w_1 \right\rangle \right\} = -V_0
\end{aligned} \tag{23}$$

and

$$\begin{aligned}
& I_1 \left\{ \frac{k}{j\omega\mu\epsilon \sin k\Delta r} \left[\Psi(r_{m-1}; r_1, r_{1+}) - 2 \cos k\Delta r \Psi(r_m; r_1, r_2) \right. \right. \\
& \qquad \qquad \qquad \left. \left. + \Psi(r_{m+1}; r_1, r_{1+}) \right] - \left\langle Z_s(r) p_1(r), w_m \right\rangle \right\} \\
& + \sum_{n=2}^M I_n \left\{ \frac{k}{j\omega\mu\epsilon \sin k\Delta r} \left[\Psi(r_{m-1}; r_{n-}, r_{n+}) - 2 \cos k\Delta r \Psi(r_m; r_{n-}, r_{n+}) \right. \right. \\
& \qquad \qquad \qquad \left. \left. + \Psi(r_{m+1}; r_{n-}, r_{n+}) \right] - \left\langle Z_s(r) p_n(r), w_m \right\rangle \right\} \\
& \qquad \qquad \qquad = 0, m=2, 3, \dots, M
\end{aligned} \tag{24}$$

These equations may be assembled into the matrix equation

$$ZI = V$$

where

$$I = \begin{bmatrix} I_1 \\ \vdots \\ I_M \end{bmatrix}, \quad V = \begin{bmatrix} -V_0 \\ 0 \\ \vdots \\ 0 \end{bmatrix}$$

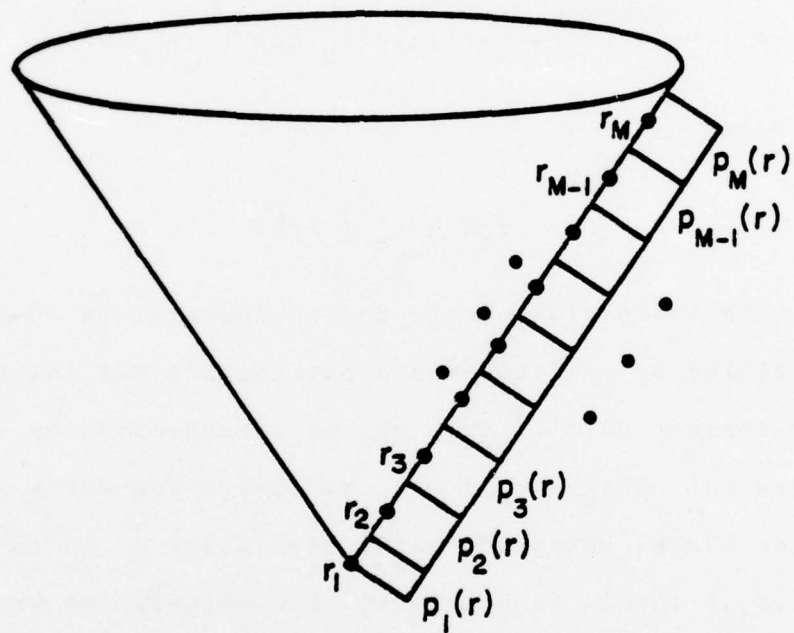


Figure 3. Pulse expansion functions for the current on the cone.

and the elements of the impedance matrix may be identified from (23) and (24). The functions $\Psi(r; r_{n-}, r_{n+})$ are defined by

$$\Psi(r; r_{n-}, r_{n+}) = \frac{\mu}{8\pi^2} \int_0^{2\pi} \int_{r_{n-}}^{r_{n+}} \frac{r}{r'} \left(\frac{e^{-jkR^+}}{R^+} - \frac{e^{-jkR^-}}{R^-} \right) dr' d\phi' \quad (25)$$

where

$$R^\pm = \sqrt{r^2 + r'^2 - 2rr'(\sin^2\theta_0 \cos\phi' \pm \cos^2\theta_0)} \quad (26)$$

and where

$$r_n^\pm = r_n \pm \Delta r/2$$

The evaluation of the double integral in (24) is simplified by analytically approximating the integration with respect to r' . This may be accomplished by noting that in general $k(r_{n+} - r_{n-}) \ll 1$, so that a few terms in a Taylor series expansion about some point r_n in the interval $[r_{n-}, r_{n+}]$ should be accurate. Accordingly, one writes

$$\begin{aligned} e^{-jkR^\pm} &= e^{-jkR_n^\pm} e^{-jk(R^\pm - R_n^\pm)} \\ &\approx e^{-jkR_n^\pm} [1 - jk(R^\pm - R_n^\pm)] \end{aligned} \quad (27)$$

where $R_n^\pm = R^\pm \Big|_{r=r_n}$. Substituting (26) into (24) and listing as a fourth argument the point about which the expansion is made, one obtains

$$\begin{aligned}
\Psi(r; r_{n-}, r_{n+}) &\approx \Psi(r; r_{n-}, r_{n+}, r_n) \\
&= \frac{\mu r}{8\pi^2} \int_0^{2\pi} \int_{r_{n-}}^{r_{n+}} \left[e^{-jkR_n^+} \left(\frac{1+jkR_n^+}{r'R^+} - \frac{jk}{r'} \right) \right. \\
&\quad \left. - e^{-jkR_n^-} \left(\frac{1+jkR_n^-}{r'R^-} - \frac{jk}{r'} \right) \right] dr' d\phi' \\
&= \frac{\mu r}{4\pi^2} \int_0^\pi \left\{ e^{-jkR_n^+} \left[\frac{1+jkR_n^+}{r} \log \left| \frac{r_{n+}(R_{n-}^+ + r - r_{n-}b^+)}{r_{n-}(R_{n+}^+ + r - r_{n+}b^+)} \right| \right. \right. \\
&\quad \left. \left. - jk\ell n \left| \frac{r_{n+}}{r_{n-}} \right| \right] \right. \\
&\quad \left. - e^{-jkR_n^-} \left[\frac{1+jkR_n^-}{r} \log \left| \frac{r_{n+}(R_{n-}^- + r - r_{n-}b^-)}{r_{n-}(R_{n+}^- + r - r_{n+}b^-)} \right| \right. \right. \\
&\quad \left. \left. - jk\ell n \left| \frac{r_{n+}}{r_{n-}} \right| \right] \right\} d\phi' \quad (28)
\end{aligned}$$

where $b^\pm = \sin^2 \theta_0 \cos \phi' \pm \cos^2 \theta_0$. In several situations, appropriate limits of the integrand of (27) need to be taken. First, when the source is the current segment at the bicone terminals, the integral (27) reduces to the simple form

$$\begin{aligned}
\Psi(r; r_1, r_{1+}) &\approx \Psi(r; r_2, r_{1+}, r_1) \\
&= \frac{\mu}{4\pi^2} \int_0^\pi e^{-jkr} (1+jkr) \log \left| \frac{R_{1+}^- + r - b^- r_{1+}}{R_{1+}^+ + r - b^+ r_{2+}} \right| d\phi' \\
&\hspace{20em} (29)
\end{aligned}$$

As the observation point r in (28) approaches the bicone terminals, $r \rightarrow r_1 = 0$, the limiting form of the integrand can be integrated. The result is

$$\Psi(r_1; r_1, r_{1+}, r_1) = \frac{\mu}{2\pi} \log(\cot \frac{\theta_0}{2}) \quad (30)$$

a very interesting result that is independent of the subdomain size at the bicone terminals. Finally, all the so-called "self terms" $\Psi(r_n; r_{n-}, r_{n+}, r_n)$, $n \neq 1$, contain an integrable singularity. In fact one easily establishes that

$$\log \left| \frac{r_{n+} (R_{n-}^+ + r - b^+ r_{n-})}{r_{n-} (R_{n+}^+ + r - b^+ r_{n+})} \right| \xrightarrow{r \rightarrow r_n} -2 \log |\phi'|$$

This singular term is then subtracted from the integrand in (27), resulting in a non-singular integrand which is then numerically integrated. The term

$$\frac{-\mu}{2\pi^2} \int_0^\pi \ln |\phi'| d\rho' = \frac{-\mu}{2\pi} (\ln \pi - 1)$$

is then added to the result to take care of the part of the integral contributed by the singularity.

SECTION IV

FORMULATION AND NUMERICAL SOLUTION OF AN INTEGRAL EQUATION FOR A BICONE WITH ENDCAPS

The formulation of the integral equation for a cone radiator over a ground plane with an endcap is considerably more complicated than that for the case when the endcap is not present. It is possible, however, to generalize the approach used for the bicone without a topcap and to transform the derivatives appearing in the equations into harmonic operators along the radial cone and topcap coordinates, as is done in Appendix B. This approach has the advantage again that testing with piecewise sinusoids allows the replacement of derivatives by a finite difference of potentials. However, to effect this transformation, an extremely complicated kernel must be used (see Appendix B) which contains many singularities other than the usual ones where source and field points coincide. While this approach has been used, it has been found to be unwieldy and rather inefficient.

The approach described here begins with the description of fields in terms of the more commonly used vector magnetic and scalar potentials expressed in terms of the cone currents and charge. However, it is found that these potentials are singular at the bicone terminals which again creates an unnecessary complication. In order to circumvent this problem, the cone and image surfaces are allowed to intersect with a

small "waist" of radius "a" (Figure 4). If "a" is very small, there should be negligible difference in the input impedance and currents found for this case and that for the limiting case of a=0. For convenience, the cone coordinates are defined with respect to the projection of the cone surface to a tip, as in Figure 4. Furthermore, the direction of the unit vector \hat{r}_t and the positive direction of corresponding vector components is taken to be towards the center of the topcap, in the direction of decreasing r_t .

The integral equations are obtained by setting the radiated field tangent to the cone surface equal to the impedance drop per unit length due to the loading:

$$-j\omega A_{r_c} - \frac{\partial \Phi}{\partial r_c} - Z_s I_c = 0, \quad a/\sin \theta_0 < r_c \leq L + a/\sin \theta_0 \quad (31)$$

$$-j\omega A_{r_t} - \frac{\partial \Phi}{\partial r_t} - Z_s I_t = 0, \quad 0 < r_t \leq L \sin \theta_0 + a \quad (32)$$

where the tangential components of magnetic vector potential, A_{r_c} and A_{r_t} , are given by

$$A_{r_p} = \frac{\mu}{8\pi^2} \left[\int_0^{2\pi} \int_{a/\sin \theta_0}^{L+a/\sin \theta_0} I_c \left(\frac{\cos \xi_{pc}^+ e^{-jkR_{pc}^+}}{R_{pc}^+} + \frac{\cos \xi_{pc}^- e^{-jkR_{pc}^-}}{R_{pc}^-} \right) dr'_c d\phi' \right. \\ \left. + \int_0^{2\pi} \int_0^{L \sin \theta_0 + a} I_t \left(\frac{\cos \xi_{pt}^+ e^{-jkR_{pt}^+}}{R_{pt}^+} + \frac{\cos \xi_{pt}^- e^{-jkR_{pt}^-}}{R_{pt}^-} \right) dr'_t d\phi' \right] \\ p = c, t \quad (33)$$

The scalar potential is given by

$$\phi = \frac{-1}{8\pi^2 j\omega\epsilon} \left[\int_0^{2\pi} \int_{a/\sin\theta_0}^{L+a/\sin\theta_0} \frac{dI_c}{dr_c} \left(\frac{e^{-jkR_{pc}^+}}{R_{pc}^+} - \frac{e^{-jkR_{pc}^-}}{R_{pc}^-} \right) dr_c' d\phi' \right. \\ \left. + \int_0^{2\pi} \int_0^{k \sin\theta_0 + a} \frac{dI_t}{dr_t} \left(\frac{e^{-jkR_{pt}^+}}{R_{pt}^+} - \frac{e^{-jkR_{pt}^-}}{R_{pt}^-} \right) dr_t^- d\phi' \right] \\ p = c, t \quad (34)$$

The currents I_c and I_t are the total linear currents on the conical and topcap surfaces, respectively, and are related to the corresponding surface current densities J_c and J_t by

$$I_c = 2\pi r_c \sin\theta_0 J_c$$

$$I_t = 2\pi r_t J_t \quad (35)$$

The distance quantities are all of the form

$$R_{pq}^{\pm} = \sqrt{r_q'^2 + 2b_{pq}^{\pm} r_q' + c_{pq}^{\pm}}, \quad p, q = c, t$$

where

$$b_{cc}^{\pm} = -r_c \sin^2\theta_0 \cos\phi' \mp r_c \cos^2\theta_0 - a \cot\theta_0 \cos\theta_0 (1 \mp 1)$$

$$c_{cc}^{\pm} = r_c^2 + a^2 \cot^2 \theta_0 (1 \mp 1)^2 - 2r_c a \cos \theta_0 \cot \theta_0 (1 \mp 1)$$

$$b_{ct}^{\pm} = -r_c \sin \theta_0 \cos \phi'$$

$$c_{ct}^{\pm} = r_c^2 - 2r_c \cos \theta_0 (a \cot \theta_0 \pm L \cos \theta_0) + (a \cot \theta_0 \pm L \cos \theta_0)^2$$

$$b_{tc}^{\pm} = \mp L \cos^2 \theta_0 - a \cos \theta_0 \cot \theta_0 - r_t \sin \theta_0 \cos \phi'$$

$$c_{tc}^{\pm} = r_t^2 + (L \cos \theta_0 \pm a \cot \theta_0)^2$$

$$b_{tt}^{\pm} = -r_t \cos \phi'$$

$$c_{tt}^{\pm} = r_t^2 + L^2 \cos^2 \theta_0 (1 \mp 1)^2$$

The angles between the source current elements and the tangential component of electric field at the observation point are determined by

$$\cos \xi_{cc}^{\pm} = \pm \cos \phi' \sin^2 \theta_0 + \cos^2 \theta_0$$

$$\cos \xi_{ct}^{\pm} = \mp \sin \theta_0 \cos \phi'$$

$$\cos \xi_{tt}^{\pm} = \pm \cos \phi'$$

$$\cos \xi_{tc}^{\pm} = \mp \cos \phi' \sin \theta_0$$

It is convenient to choose as testing functions the pulse functions p_n shown in Figure 5. Thus, testing (31) with p_1 results in

$$-j\omega \langle A_{r_c}, p_1 \rangle - \left\langle \frac{\partial \phi}{\partial r_c}, p_1 \right\rangle - \langle Z_s I_c, p_1 \rangle = 0$$

Upon integrating by parts in the central term, and noting that A_{r_c} is slowly varying over the interval and hence may be approximated by $A_{r_c}(r_{c1})$, one obtains

$$-j\omega A_{r_c}(r_{c1}) \frac{\Delta r_c}{2} - [(\phi(r_{c1} + \Delta r_c/2) - \phi(r_{c1}))] - \langle Z_s I_c, p_1 \rangle = 0$$

But $\phi(r_{c1})$ is just the bicone terminal voltage V_0 with respect to the ground plane. Hence,

$$-j\omega A_{r_c}(r_{c1}) \Delta r_c - 2\phi(r_{c1} + \Delta r_c/2) - 2\langle Z_s I_c, p_1 \rangle = -2V_0 \quad (36)$$

For the remaining testing functions on the cone, testing of (31), integration by parts on the scalar potential term and approximation of the vector potential by its value at the center of the pulse yields

$$-j\omega \Delta r_c A_{r_c}(r_{cm}) - [\phi(r_{cm} + \Delta r_c/2) - \phi(r_{cm} - \Delta r_c/2)] - \langle Z_s I_c, p_m \rangle = 0, \quad m = 2, 3, \dots, N_c - 1 \quad (37)$$

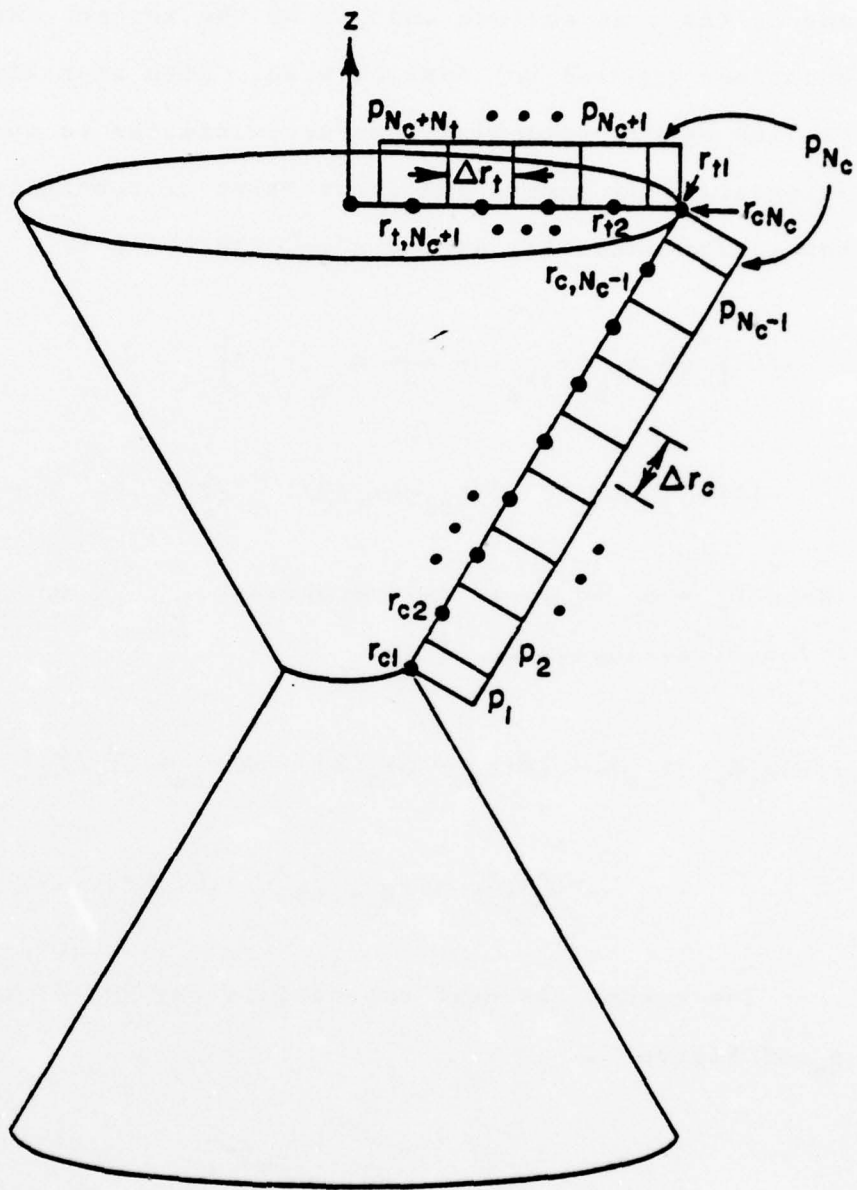


Figure 5. Pulse expansion and testing functions.

At the edge, the testing pulse consists of two parts, one on the cone surface and one on the topcap. Hence, both equations (31) and (32) must be used. With approximations on the two vector potential components similar to that above, integration by parts, and enforcement of continuity of the scalar potential at the edge, one obtains

$$-j\omega \left[\frac{\Delta r_c}{2} A_{r_c}(r_{cN_c}) + \frac{\Delta r_t}{2} A_{r_t}(r_{t1}) \right] - [\phi(r_{cN_c} - \Delta r_c/2) - \phi(r_{t1} + \Delta r_t/2)] - \langle Z_s I_r, P_{N_c} \rangle = 0 \quad (38)$$

where $I_r = I_c$ or I_t as is appropriate. On the topcap, one has, analogous to (37),

$$-j\omega \Delta r_t A_{r_t}(r_{tm}) - [\phi(r_{tm} - \Delta r_t/2) - \phi(r_{tm} + \Delta r_t/2)] - \langle Z_s I_t, P_{N_c - 1 + m} \rangle = 0, m=2, \dots, N_t + 1 \quad (39)$$

The current is next expanded in the set of pulse functions p_n of Figure 5,

$$I_c(r_c) \approx \sum_{n=1}^{N_c} I_n p_n(r_c) \quad (40)$$

$$I_t(r_t) = \sum_{n=N_c}^{N_c + N_t} I_n p_n(r_t) \quad (41)$$

Note that the current I_{N_c} at the edge of the cone is the same on both the cone and the topcap surfaces. The derivatives of the currents above are approximated by a finite difference of adjacent current pulses which is then assumed to be expanded in its own set of "charge" pulses (see Figure 6);

$$\frac{dI_c}{dr_c} \approx \sum_{n=1}^{N_c-1} \left(\frac{I_{n+1} - I_n}{\Delta r_c} \right) p_n^+(r_c) \quad (42)$$

$$\frac{dI_t}{dr_t} \approx \sum_{n=N_c}^{N_c+N_t} \left(\frac{I_{n+1} - I_n}{\Delta r_t} \right) p_n^+(r_t) \quad (43)$$

where $I_{N_c+N_t+1}$ is taken to be zero.

Thus the vector potential quantities in (36)-(39) may be written as

$$\begin{aligned} A_{r_t} = \frac{\mu}{8\pi^2} \left\{ I_1 \Psi_{pc}(r_p, r_{c1}, r_{c1} + \Delta r_c/2) \right. \\ + \sum_{n=2}^{N_c-1} I_n \Psi_{pc}(r_p, r_{cn} - \Delta r_c/2, r_{cn} + \Delta r_c/2) \\ + I_{N_c} [\Psi_{pc}(r_p, r_{cN_c} - \Delta r_c/2, r_{cN_c}) + \Psi_{pt}(r_p, r_{t1}, r_{t1} + r_t/2)] \\ \left. + \sum_{n=N_c+1}^{N_c+N_t} I_n \Psi_{pt}(r_p, r_{t,n+1-N_c} - \Delta r_t/2, r_{t,n+1-N_c} + \Delta r_t/2) \right\} \\ p = c, t \quad (44) \end{aligned}$$

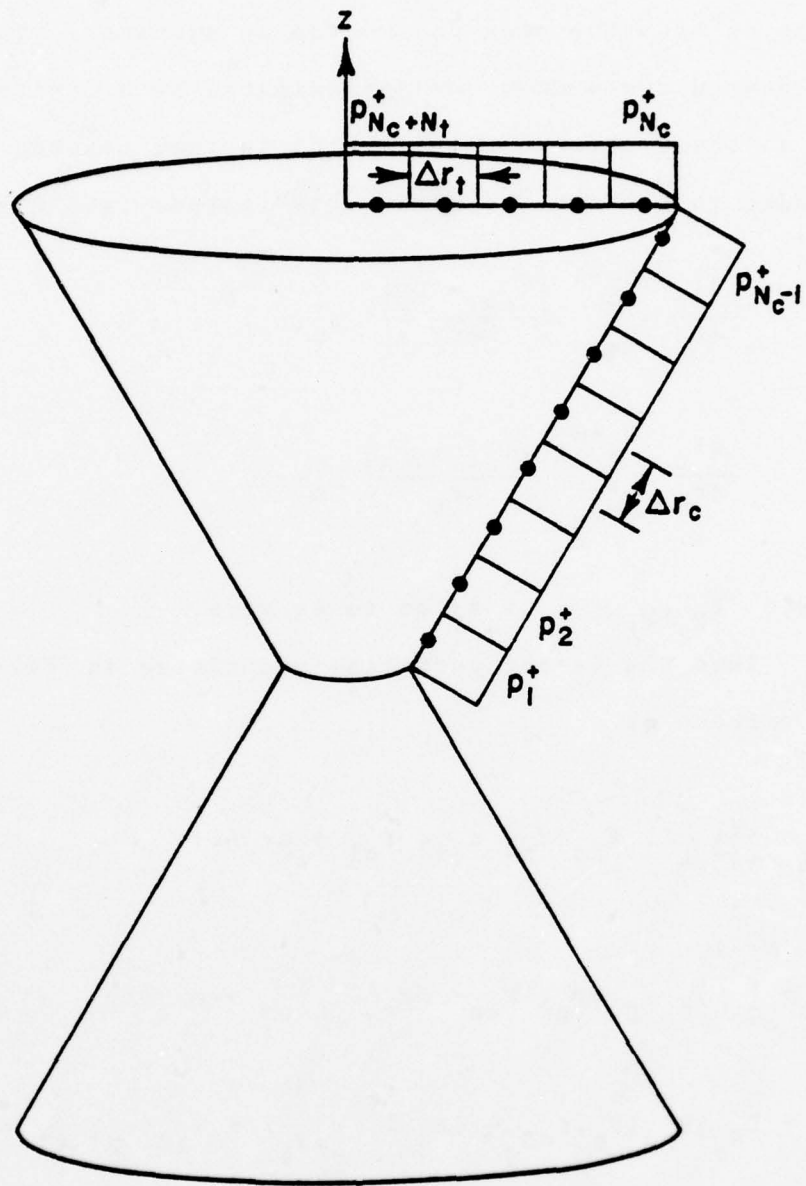


Figure 6. Pulse expansions for the charge on the cone.

and the scalar potential is

$$\phi = \frac{-1}{8\pi^2 j\omega\epsilon} \left[\sum_{n=1}^{N_c-1} \left(\frac{I_{n+1} - I_n}{\Delta r_c} \right) \psi_{pc}(r_p, r_{cn}, r_{cn} + \Delta r_c) \right. \\ \left. + \sum_{n=N_c}^{N_c+N_t} \left(\frac{I_{n+1} - I_n}{\Delta r_t} \right) \psi_{pt}(r_p, r_{t,n+1-N_c}, r_{t,n+1-N_c} + \Delta r_c) \right] \\ p = c, t \quad (45)$$

where

$$\psi_{pq}(r_p, r_{n-}, r_{n+}) = \int_0^{2\pi} \left(\cos \xi_{pq}^+ \int_{r_{n-}}^{r_{n+}} \frac{e^{-jkR_{pq}^+}}{R_{pq}^+} dr' \right. \\ \left. + \cos \xi_{pq}^- \int_{r_{n-}}^{r_{n+}} \frac{e^{-jkR_{pq}^-}}{R_{pq}^-} dr' \right) d\phi' \\ p, q = c, t \quad (46)$$

and

$$\psi_{pq}(r_p, r_{n-}, r_{n+}) = \int_0^{2\pi} \int_{r_{n-}}^{r_{n+}} \left(\frac{e^{-jkR_{pq}^+}}{R_{pq}^+} \right. \\ \left. - \frac{e^{-jkR_{pq}^-}}{R_{pq}^-} \right) dr' d\phi' \\ p, q = c, t \quad (47)$$

The inner integrals in (46) and (47) can be approximately analytically integrated. They are all of the form

$$\int_{r_{n-}}^{r_{n+}} \frac{e^{-jkR}}{R} dr' \quad (48)$$

where R is of the form

$$R = \sqrt{r'^2 + 2r'b + c} \quad (49)$$

Since the range of integration $[r_{n-}, r_{n+}]$ is small compared to a wavelength, it is appropriate to expand e^{-jkR} in a Taylor series about some point R_n which is the distance from the observation point to a point r_n in the interval $[r_{n-}, r_{n+}]$. Thus,

$$\begin{aligned} e^{-jkR} &= e^{-jk(R-R_n)} e^{-jkR_n} \\ &= e^{-jkR_n} [\cos k(R-R_n) - j \sin k(R-R_n)] \\ &\approx e^{-jkR_n} \left[1 - \frac{k^2(R-R_n)^2}{2} - jk(R-R_n) \right. \\ &\quad \left. + jk^3(R-R_n)^3/6 \right] \end{aligned}$$

The error in the real and imaginary parts is less than

$$\text{Max}_{r' \in [r_{n-}, r_{n+}]} \frac{k^4 (R-R_n)^4}{24} \leq \frac{k^4 (\Delta r/2)^4}{24}$$

where Δr is the subdomain size. For five subdomains per wavelength ($\Delta r/\lambda = 1/5$), this results in a maximum error of less than 1% in both the real and imaginary parts of the integrand. The resulting integral should indeed be much more accurate than this. With this approximation,

$$\int_{r_{n-}}^{r_{n+}} \frac{e^{-jkR}}{R} dr' \approx e^{-jkR_n} (I_1 - jI_2)$$

where

$$\begin{aligned} I_1 &= \int_{r_{n-}}^{r_{n+}} \frac{1 - k^2 (R - R_n)^2 / 2}{R} dr' \\ &= \left(1 - \frac{k^2 R_n^2}{2} \right) \ell_n \left| \frac{R_{n+} + r_{n+} + b}{R_{n-} + r_{n-} + b} \right| + k^2 R_n (r_{n+} - r_{n-}) \\ &\quad - k^2 \left[\frac{r_{n+} + b}{2} R_{n+} - \frac{r_{n-} + b}{2} R_{n-} + \frac{c-b}{2} \ell_n \left| \frac{R_{n+} + r_{n+} + b}{R_{n-} + r_{n-} + b} \right| \right] \end{aligned}$$

and where

$$\begin{aligned} I_2 &= \int_{r_{n-}}^{r_{n+}} \frac{k(R - R_n) - k^3 (R - R_n)^3 / 6}{R} dr' \\ &= (-k R_n + k^3 R_n^3 / 6) \ell_n \left| \frac{R_{n+} + r_{n+} + b}{R_{n-} + r_{n-} + b} \right| + (k - k^3 R_n^2 / 2) (r_{n+} - r_{n-}) \end{aligned}$$

$$\begin{aligned}
& + \frac{k^3 R_n}{2} \left[\frac{r_{n+} + b}{2} R_{n+} - \frac{r_{n-} + b}{2} R_{n-} + \frac{(c-b)^2}{2} \ell_n \left| \frac{R_{n+} + r_{n+} + b}{R_{n-} + r_{n-} + b} \right| \right] \\
& - \frac{k^3}{6} \left[\frac{r_{n+}^3 - r_{n-}^3}{3} - b(r_{n+}^2 - r_{n-}^2) + c(r_{n+} - r_{n-}) \right]
\end{aligned}$$

Combining these results, one has, finally,

$$\begin{aligned}
& \int_{r_{n-}}^{r_{n+}} \frac{e^{-jkR}}{R} dr' \approx \\
& e^{-jkR_n} \left\{ \left[1 + jkR_n - \frac{k^2 R_n^2}{2} - j \frac{k^3 R_n^3}{6} \right. \right. \\
& \quad - \left. \left(\frac{k^2}{2} + j \frac{k^3 R_n}{2} \right) \left(\frac{c-b}{2} \right) \right] \ell_n \left| \frac{R_{n+} + r_{n+} + b}{R_{n-} + r_{n-} + b} \right| \\
& \quad - \frac{1}{4} (k^2 + jk^3 R_n) [(r_{n+} + b)R_{n+} - (r_{n-} + b)R_{n-}] \\
& \quad + \frac{jk^3}{6} \left[\frac{r_{n+}^3 + r_{n-}^3}{3} + b(r_{n+}^2 - r_{n-}^2) \right] \\
& \quad \left. + \left(-jk + k^2 R_n + j \frac{k^3 R_n^2}{2} + j \frac{k^3 c}{6} \right) (r_{n+} - r_{n-}) \right\} \quad (50)
\end{aligned}$$

Equation (50) is singular in ϕ' if the observation point is in the interval $[r_{n-}, r_{n+}]$. Hence, the integrals in (46) and

(47) need to be evaluated by subtracting the singularity from the integrand and adding its integral to the numerically determined integral. If r_n is in the interior of the interval, $r_{n-} < r_n < r_{n+}$, (50) behaves like $-2\ell n|\phi'|$ near $\phi' = 0$; if $r_n = r_{n-}$ or $r_n = r_{n+}$, (50) behaves like $-\ell n|\phi'|$. The details of the procedure parallels that described at the end of Section III.

SECTION V
NUMERICAL RESULTS AND CONCLUSIONS

This section describes numerical results obtained from the computer code developed from the theory described in Section IV. The resulting code was written to model the cone with or without a topcap. Hence, results from this general code could be checked against those obtained from the code based on the methods of Section III for the cone without a topcap. For narrow cone angles, the calculated input impedance for unloaded cones for various frequencies was also compared to the theory of Schelkunoff [5] and found to be in very good agreement. Results from the general code for moderate cone angles were also compared with those computed by the method of Appendix B, which includes the effects of the topcap. These comparisons were made to validate the consistency of the various approaches and to compare with existing data. It was also established that the input reactance at low frequencies could be used to check the static capacitance calculated in the companion report [1] for both the loaded and unloaded case. Finally, it was verified that the computed results were almost independent of the choice of the waist radius, a , of Section III, provided a was chosen small enough.

All the data in this section pertain to a conical antenna with a vertical height of 40 meters and a cone angle of $\theta_0 = 42.26^\circ$. These parameters translate to a cone slant height of 54.05 meters and correspond approximately to the cone considered in [6]. The locations and values of the lumped resistive loads used are listed in Table 1 and are taken from [6].

Figures 7-10 illustrate the current distribution on the cone at a frequency of 825 KHz, approximately the first resonant frequency of the unloaded structure. Figures 11-14 illustrate the same results at 1.375 MHz, approximately half-way between first and second resonance of the unloaded structure (see Figures 15 and 16). Two features of the current distributions are notable. First, the edge condition [7], which requires that the current at the edge has infinite slope, and the continuity equation relating current and charge, which requires that the total current approach zero with zero slope at the center of the topcap, combine to limit the amount of current the topcap can support. Secondly, the loading, which increases to a maximum at the edge, further limits current flow on the topcap.

Figures 15-18 illustrate the variation with frequency of the input impedance of the conical structure for the various loading and topcap configurations. Again, the influence of the topcap is found to be negligible. The absence of

Table 1. Positions and values of loading resistors on the cone.

ARC LENGTH ALONG THE CONE GENERATOR (METERS)	RESISTANCE (OHMS)
12.17	4.69
14.34	7.17
16.90	9.06
19.93	11.74
23.54	15.43
27.73	20.82
32.59	30.36
38.41	50.38
45.31	114.88
53.43	114.88
63.15	100.00
72.25	100.00
81.35	100.00

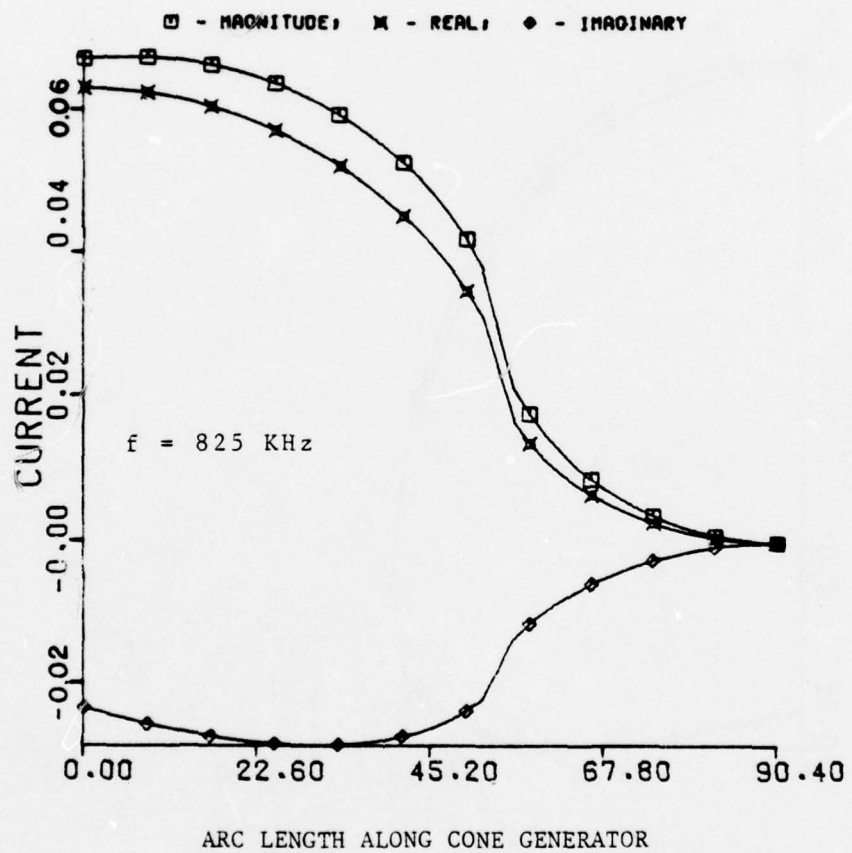
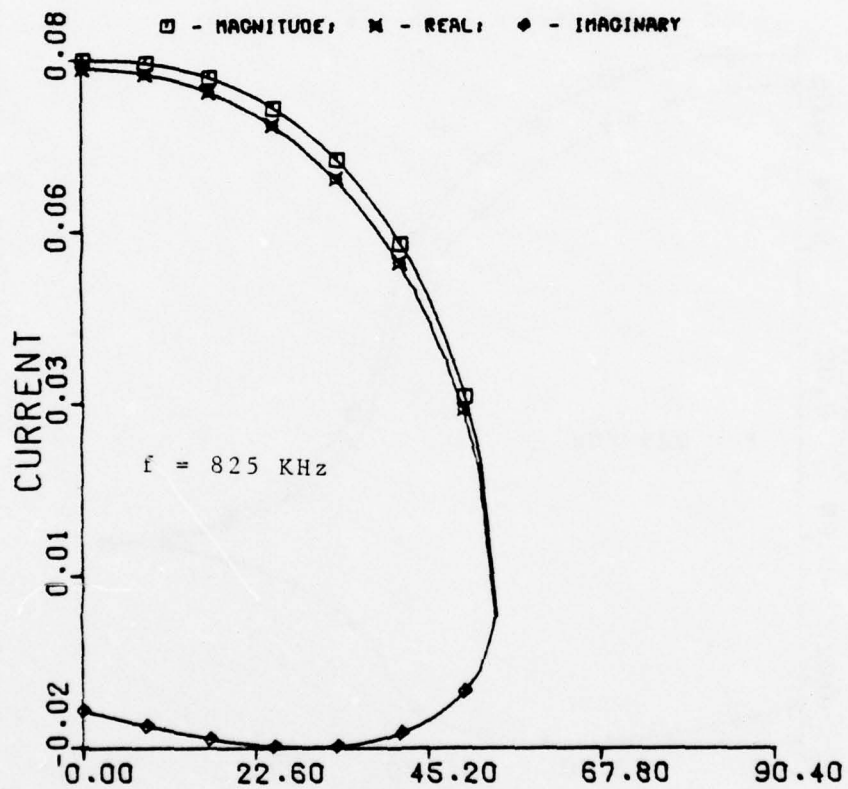


Figure 7. Current on unloaded cone with topcap, $L=54.05\text{m}$, $\theta_0 = 42.26^\circ$, $V_0 = 1 \text{ Volt}$, $f = 825 \text{ KHz}$.



ARC LENGTH ALONG CONE GENERATOR

Figure 8. Current on unloaded cone without topcap,
 $L=54.05\text{m}$, $\theta_0 = 42.26^\circ$, $V_0 = 1 \text{ Volt}$, $f = 825 \text{ KHz}$.

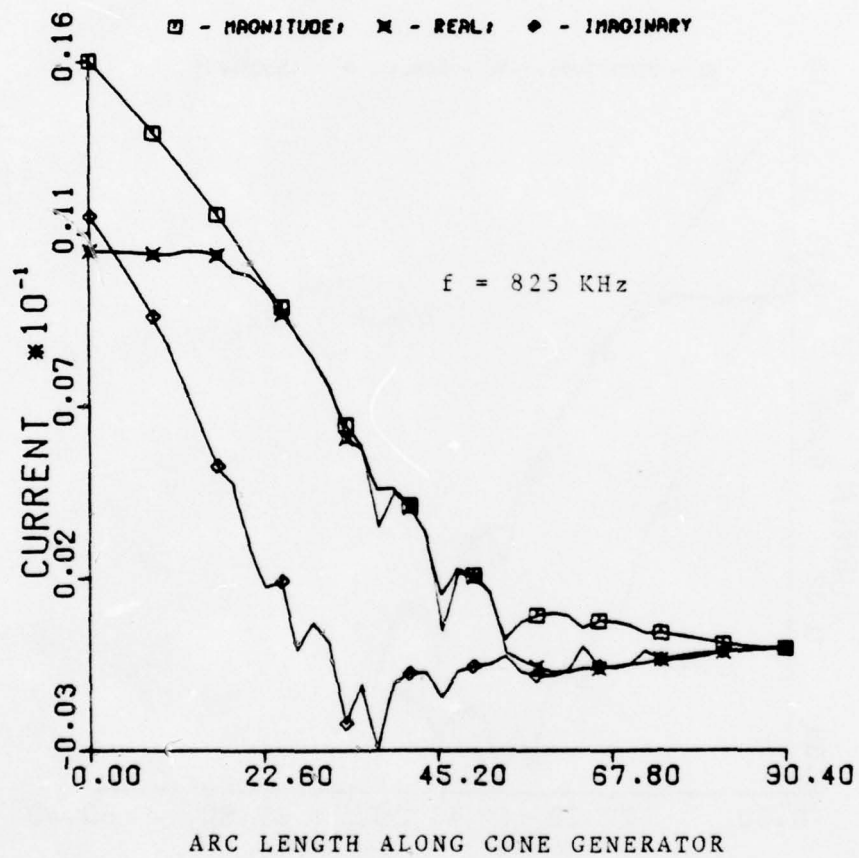


Figure 9. Current on loaded cone with topcap, $L=54.05\text{m}$, $\theta_0 = 42.26^\circ$, $V_0 = 1 \text{ Volt}$, $f = 825 \text{ KHz}$.

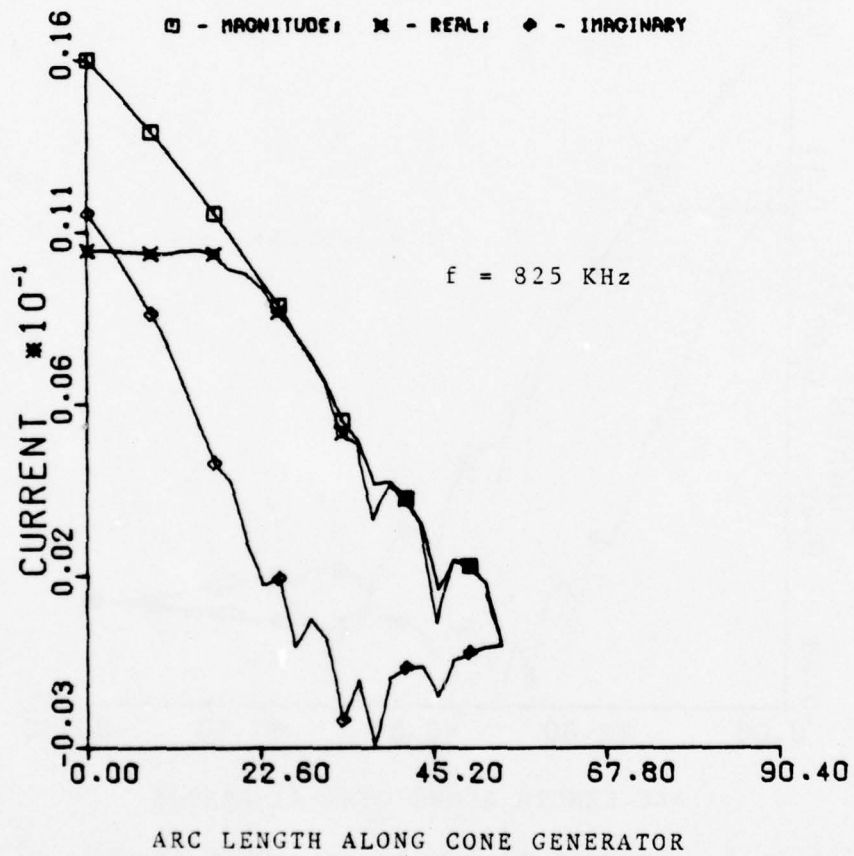


Figure 10. Current on loaded cone without topcap,
 $L=54.05\text{m}$, $\theta_0 = 42.26^\circ$, $V_0 = 1 \text{ Volt}$,
 $f = 825 \text{ MHz}$.

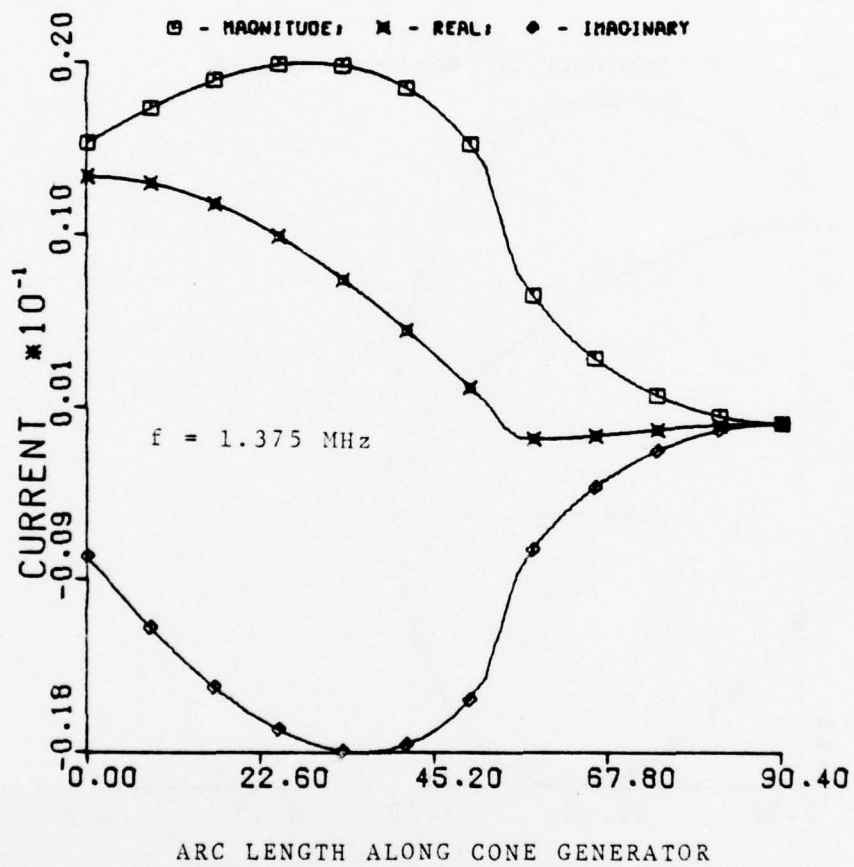


Figure 11. Current on unloaded cone with topcap, $L=54.05\text{m}$, $\theta_0 = 42.26^\circ$, $V_0 = 1 \text{ Volt}$, $f = 1.375 \text{ MHz}$.

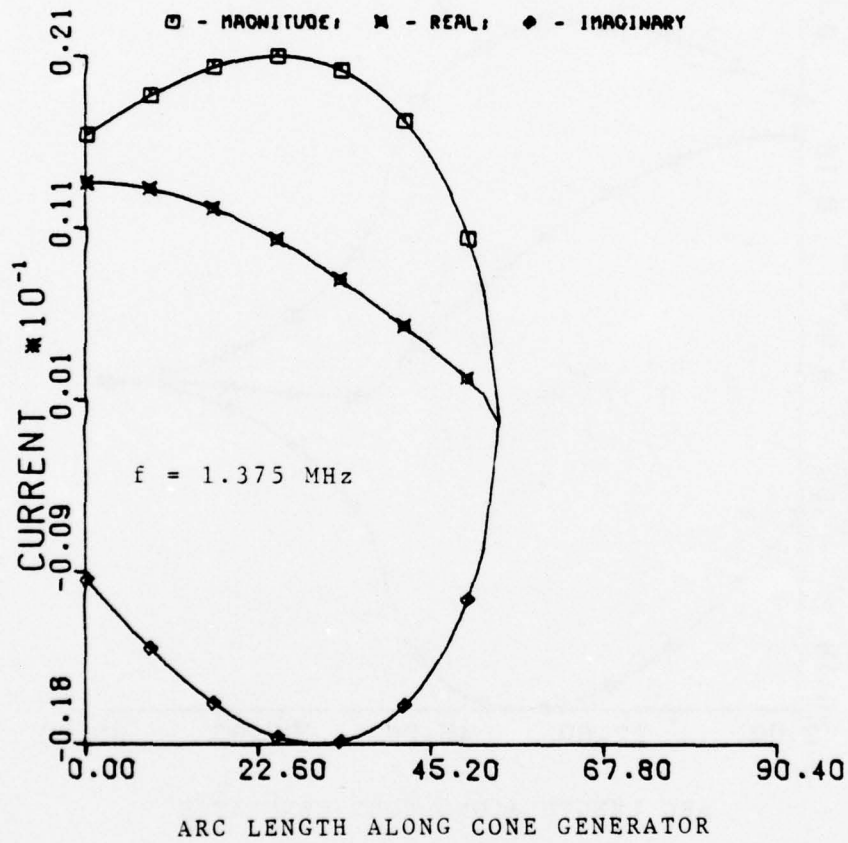


Figure 12. Current on unloaded cone without topcap, $L=54.05\text{m}$, $\theta_0 = 42.26^\circ$, $V_0 = 1 \text{ Volt}$, $f = 1.375 \text{ MHz}$.

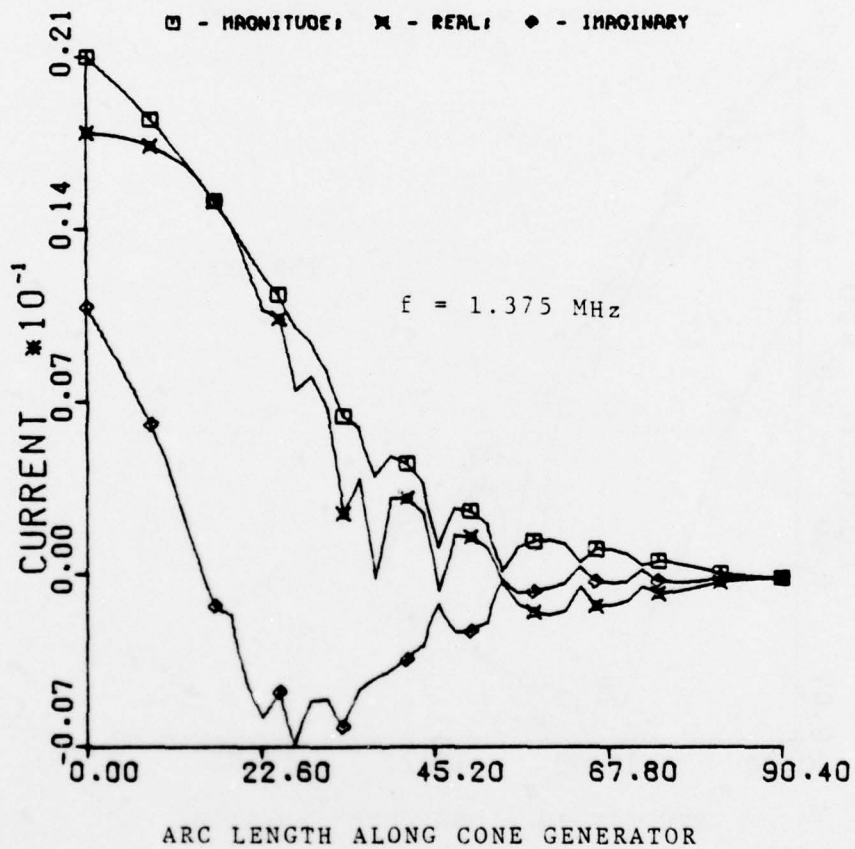


Figure 13. Current on loaded cone with topcap, $L=54.05\text{m}$, $\theta_0 = 42.26^\circ$, $V_0 = 1 \text{ Volt}$, $f = 1.375 \text{ MHz}$.

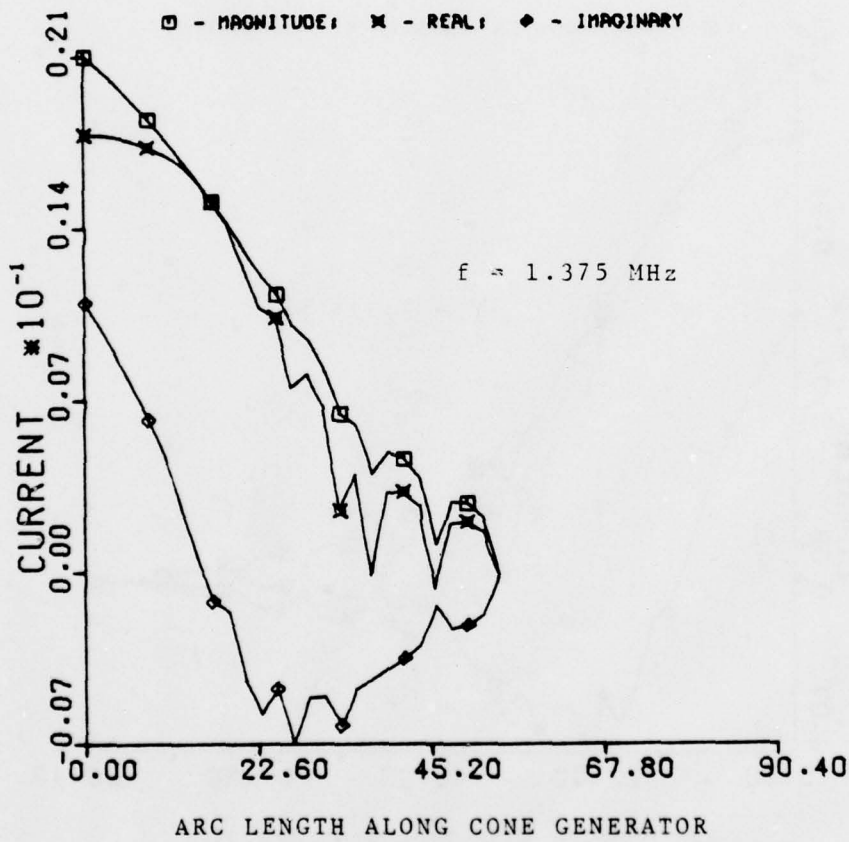


Figure 14. Current on loaded cone without topcap,
 $L=54.05\text{m}$, $\theta_0 = 42.26^\circ$, $V_0 = 1 \text{ Volt}$,
 $f = 1.375 \text{ MHz}$.

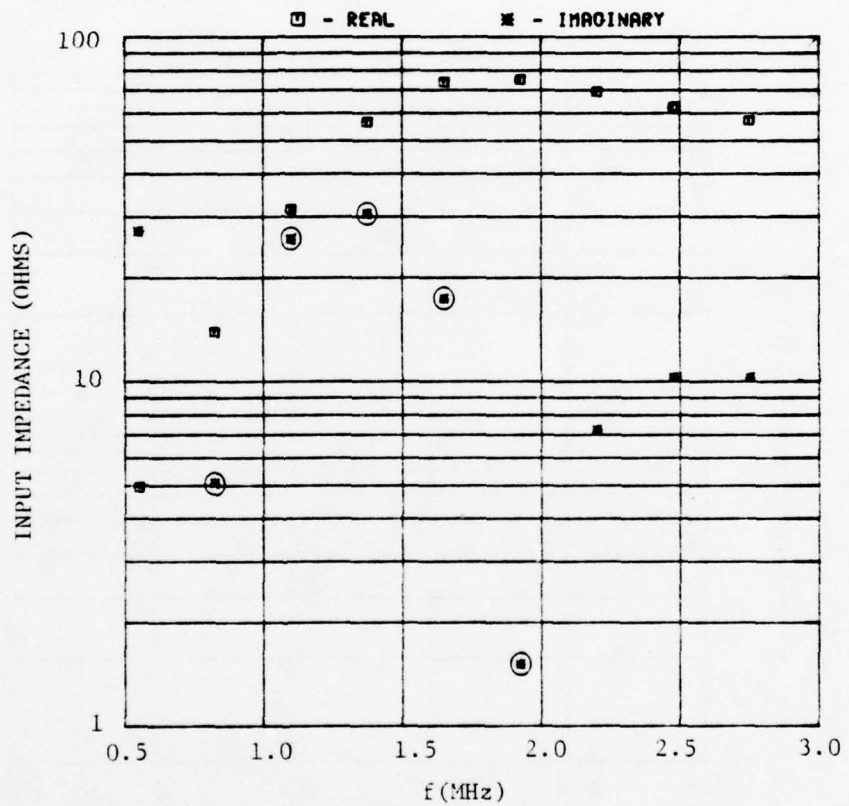


Figure 15. Input impedance of unloaded cone with topcap, $L=54.05m$, $\theta_0 = 42.26^\circ$. Encircled values of imaginary part are positive.

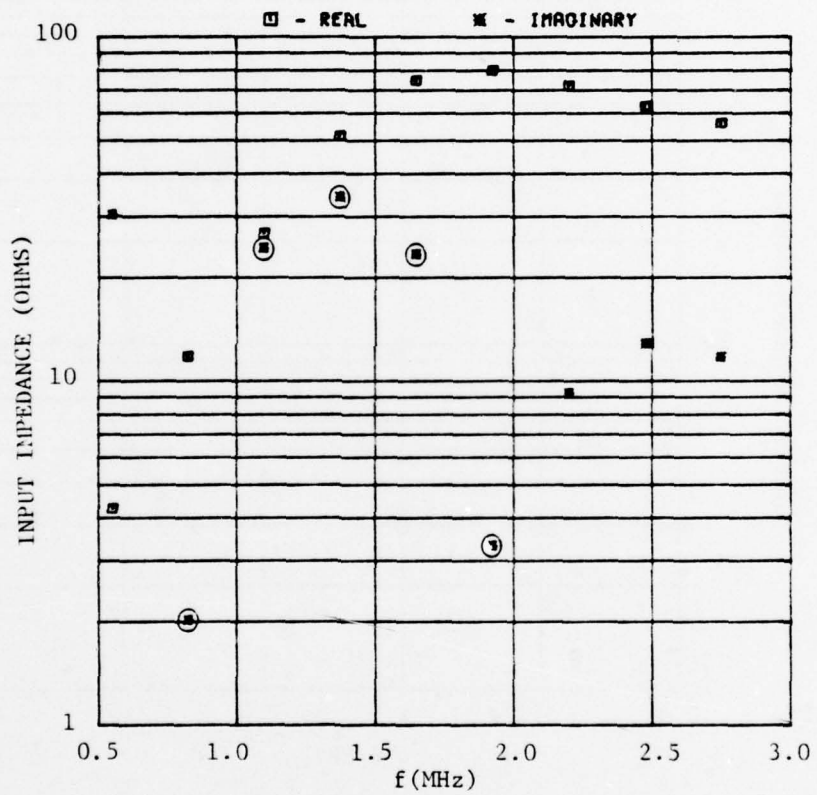


Figure 16. Input impedance of unloaded cone without topcap, $L=54.05\text{m}$, $\theta_0 = 42.26^\circ$. Encircled values of imaginary part are positive.

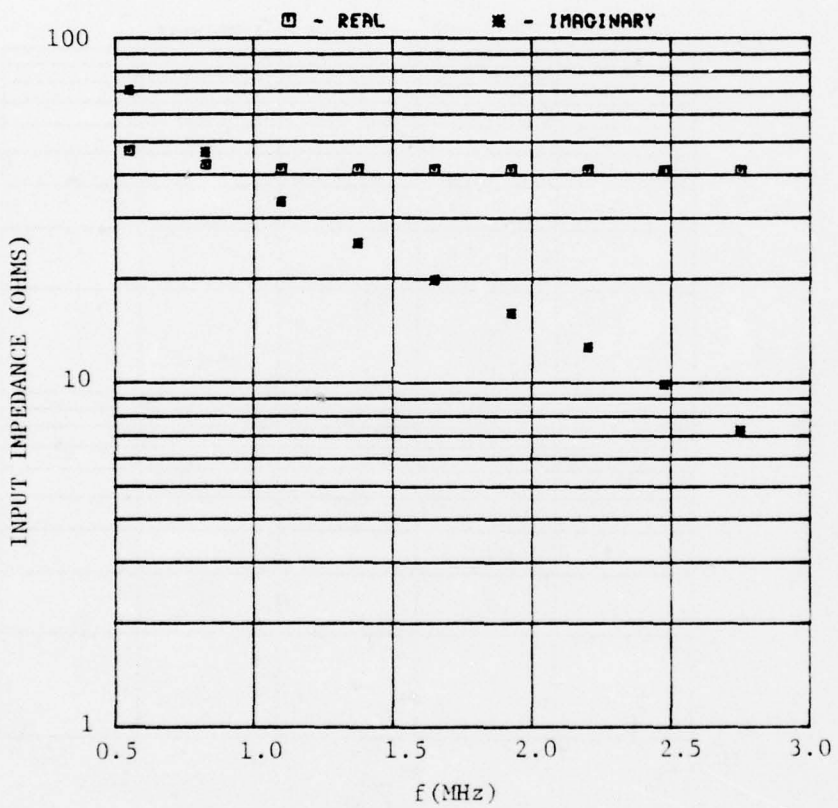


Figure 17. Input impedance of loaded cone with topcap, $L=54.05\text{m}$, $\theta_0 = 42.26^\circ$. Imaginary values are negative.

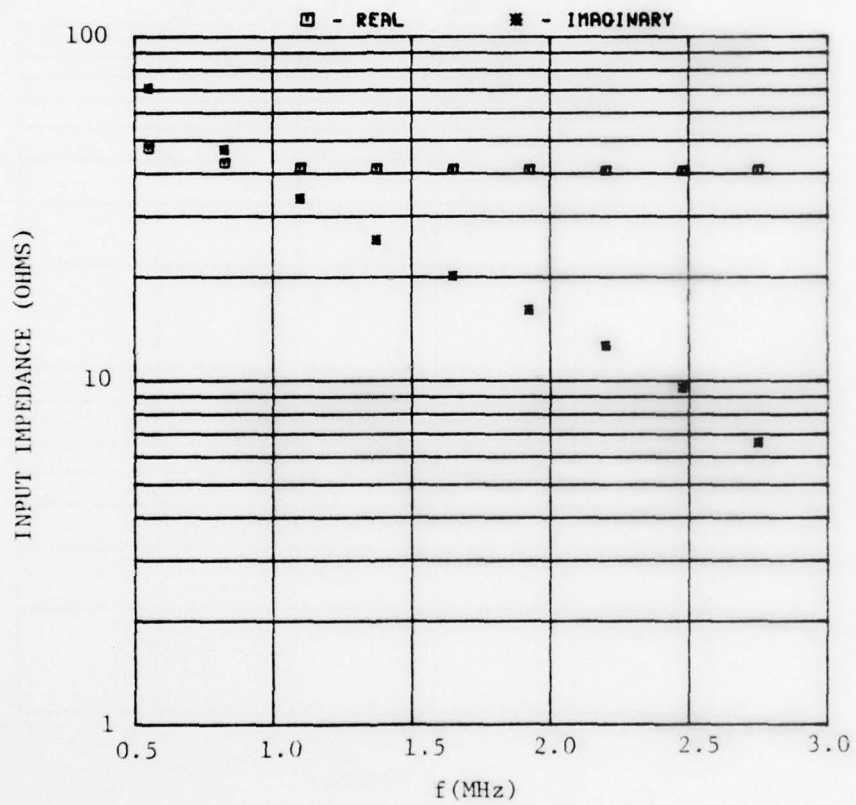


Figure 18. Input impedance of loaded cone without topcap, $L=54.05m$. $\theta_0 = 42.26^\circ$. Imaginary values are negative.

resonances in the loaded case can be attributed to the effectiveness of the resistive loading in eliminating reflections from the cone edge which would result in standing waves on the structure. However, one would also expect the bicone input impedance to approach a value of $56.5 + j 0.0$ ohms, the input impedance of an infinite bicone of the same cone angle, with increasing frequency. Instead, the impedance in Figures 17 and 18 seems to be approaching a value nearer $40 + j 0.0$ ohms. Computations at higher frequencies indicate that the real part of the impedance begins to increase at about 3.0 MHz and at 10 MHz is at about $60 + j 8$ ohms, slightly above the infinite bicone impedance. Repeating the computations with the continuous loading function described in [6] did indeed result in an input impedance which monotonically approached that of an infinite bicone. Thus, it appears that some further adjustment in the values of the discrete loading resistors might be made in order to more closely approximate the impedance behavior of the infinite bicone.

Radiation patterns in the near-field region of the loaded structure with a topcap ($r = 100$ meters and the frequency is 550 KHz) are shown in Figures 19-21. Figures 22-24 give the corresponding patterns in the far field ($r = 10^4$ meters). For comparison, far field patterns for the unloaded structure are illustrated in Figures 25-27.

Although resources did not permit a time-domain analysis of the response of the structure, such a study, which could include a simple equivalent circuit model of the pulser,

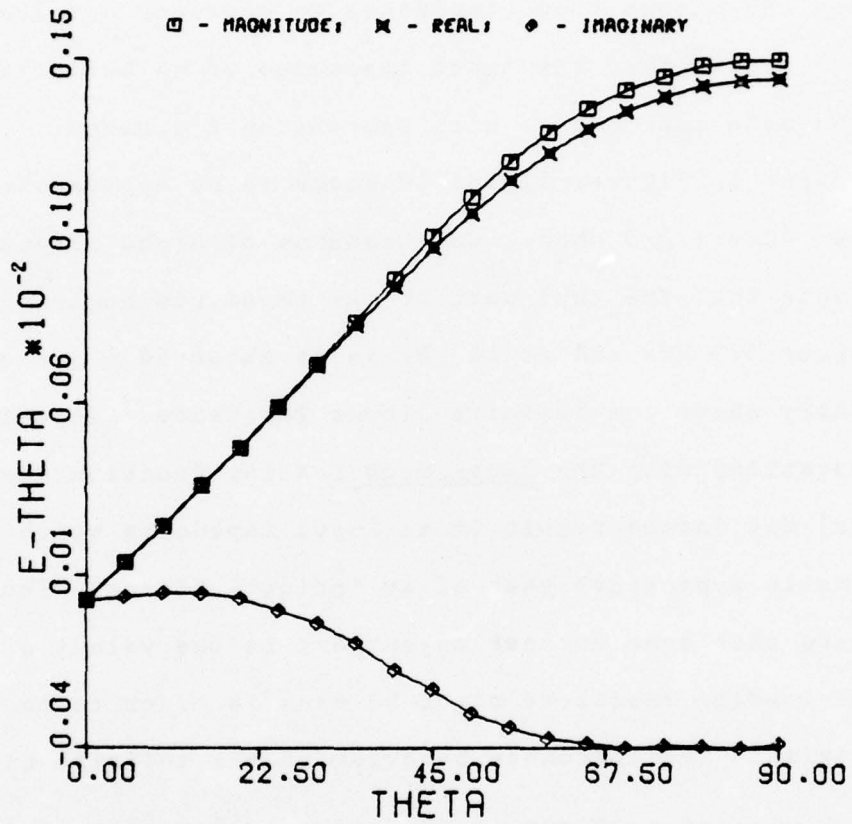


Figure 19. E_{θ} radiation pattern for loaded cone with topcap, $L=54.05\text{m}$, $\theta_0 = 42.26^\circ$, $V_0=1$ Volt, $f = 550$ KHz, $r = 100\text{m}$.

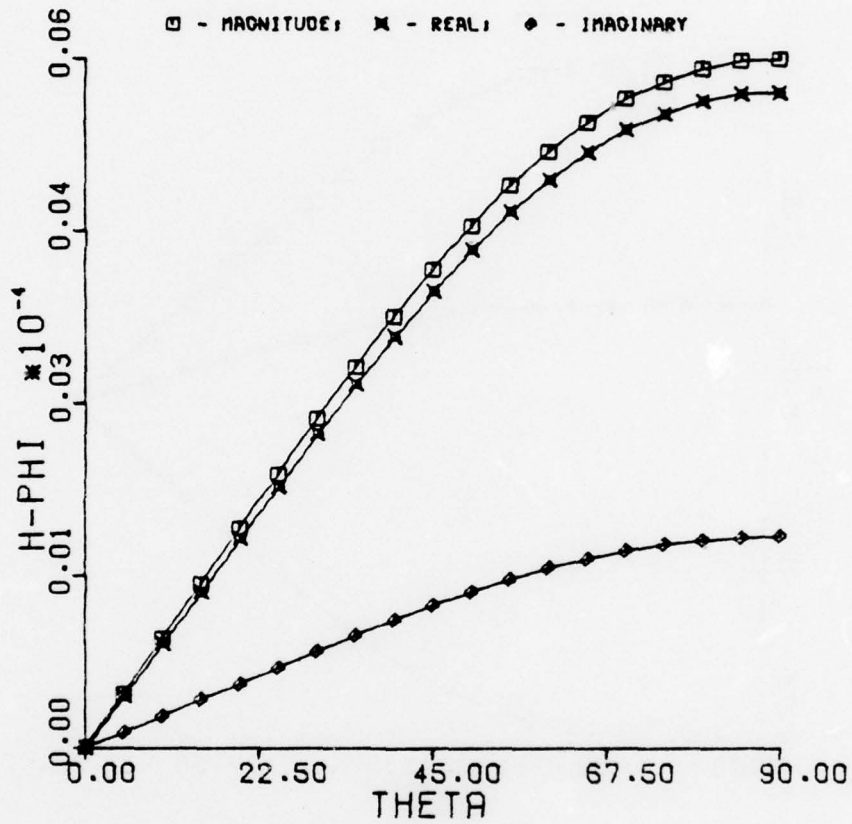


Figure 20. H_{ϕ} radiation pattern for loaded cone with topcap, $L=54.05m$, $\theta_0 = 42.26^\circ$, $V_0 = 1$ Volt, $f = 550$ KHz, $r = 100m$.

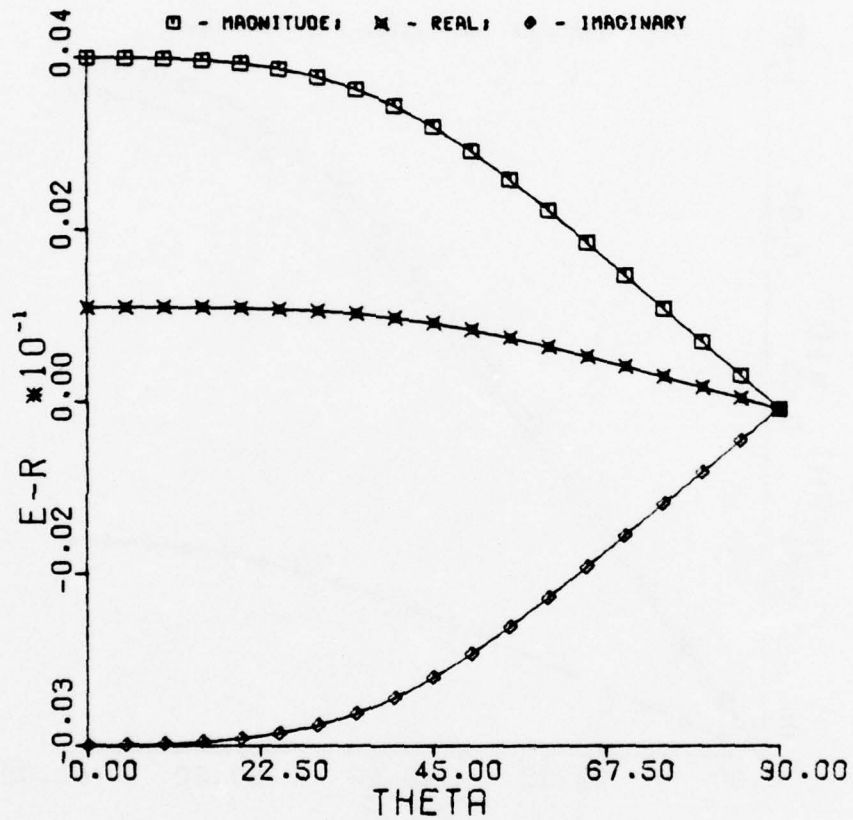


Figure 21. E_r radiation pattern for loaded cone with topcap, $L=54.05\text{m}$, $\theta_0 = 42.26^\circ$, $V_0 = 1$ Volt, $f = 550$ KHz, $r = 100\text{m}$.

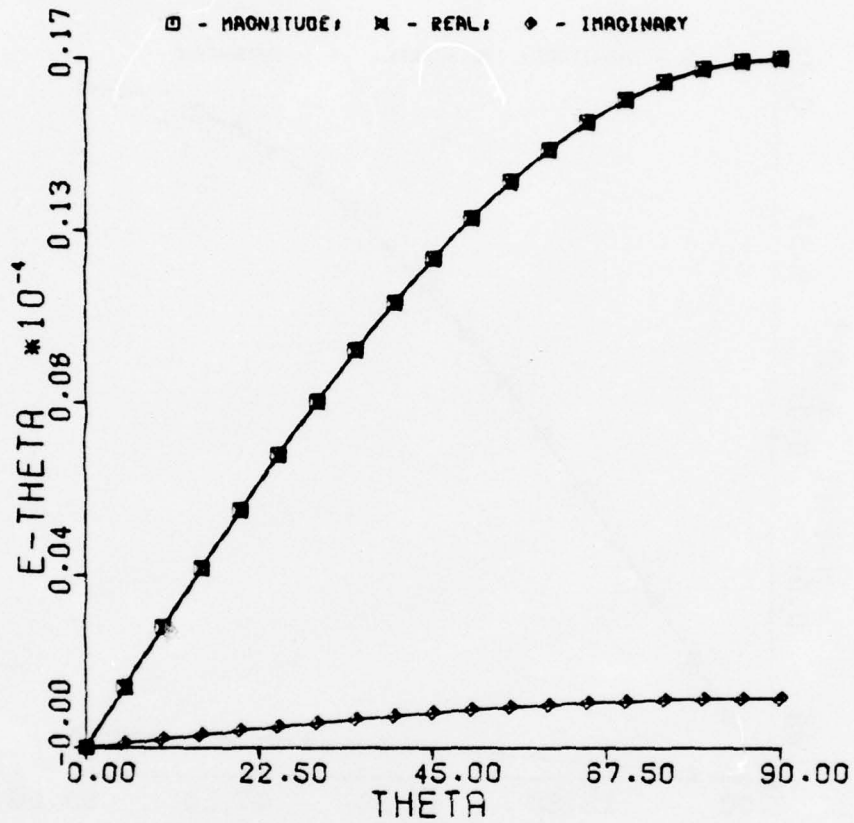


Figure 22. E_{θ} radiation pattern for loaded cone with topcap, $L=54.05\text{m}$, $\theta_0 = 42.26^\circ$, $V_0 = 1 \text{ Volt}$, $f = 550 \text{ KHz}$, $r = 10^4\text{m}$.

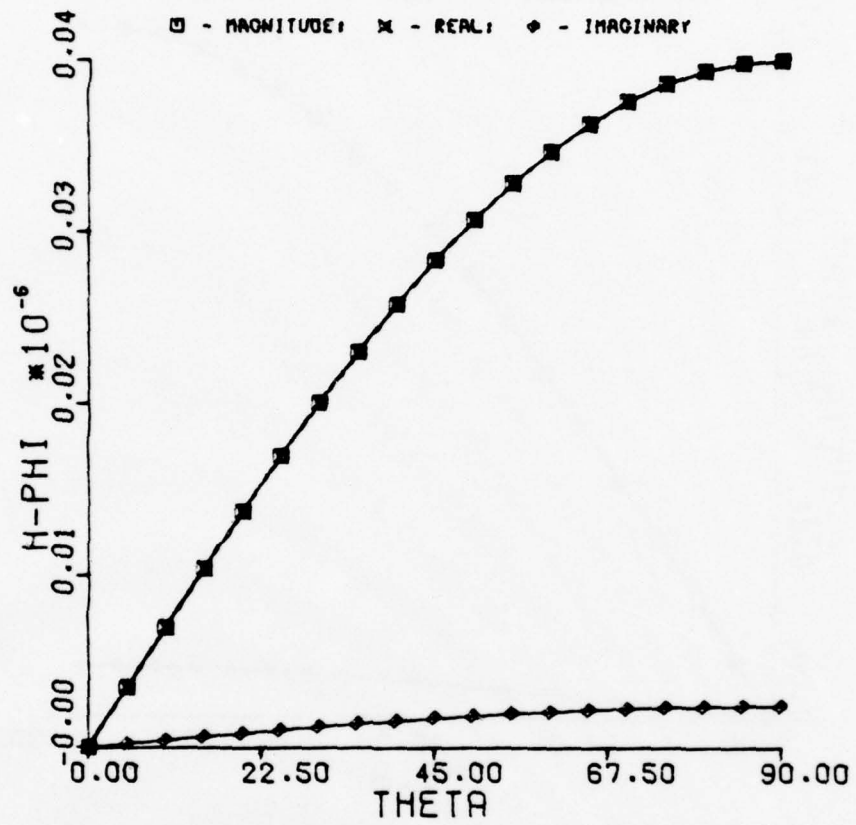


Figure 23. H_{ϕ} radiation pattern for loaded cone with topcap, $L=54.05\text{m}$, $\theta_0 = 42.26^\circ$, $V_0 = 1 \text{ Volt}$, $f = 550 \text{ KHz}$, $r = 10^4\text{m}$.

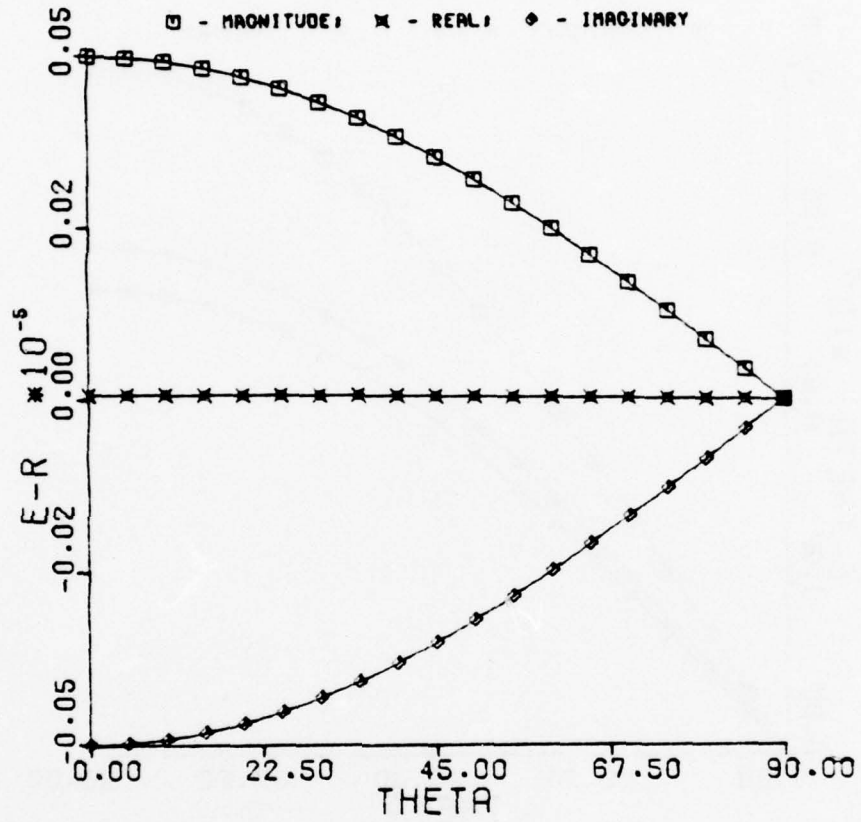


Figure 24. E_r radiation pattern for loaded cone with topcap, $L=54.05m$, $\theta_0 = 42.26^\circ$, $V_0 = 1$ Volt, $f = 550$ KHz, $r = 10^4m$.

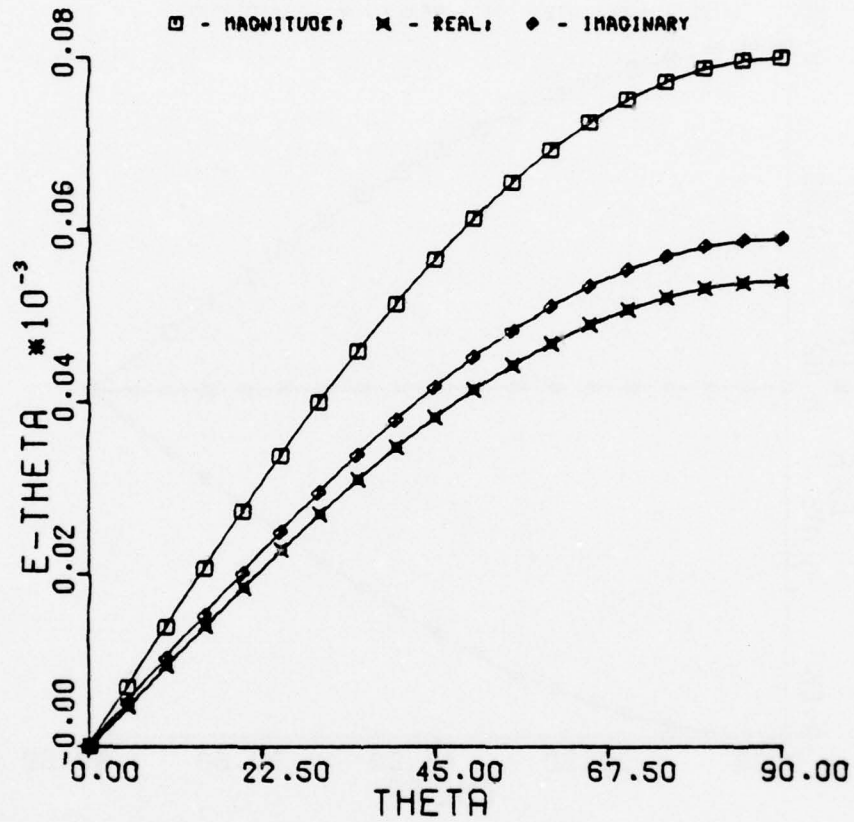


Figure 25. E_{θ} radiation pattern for unloaded cone with topcap, $L=54.05m$, $\theta_0 = 42.26^\circ$, $V_0 = 1$ Volt, $f = 550$ KHz, $r = 10^4m$.

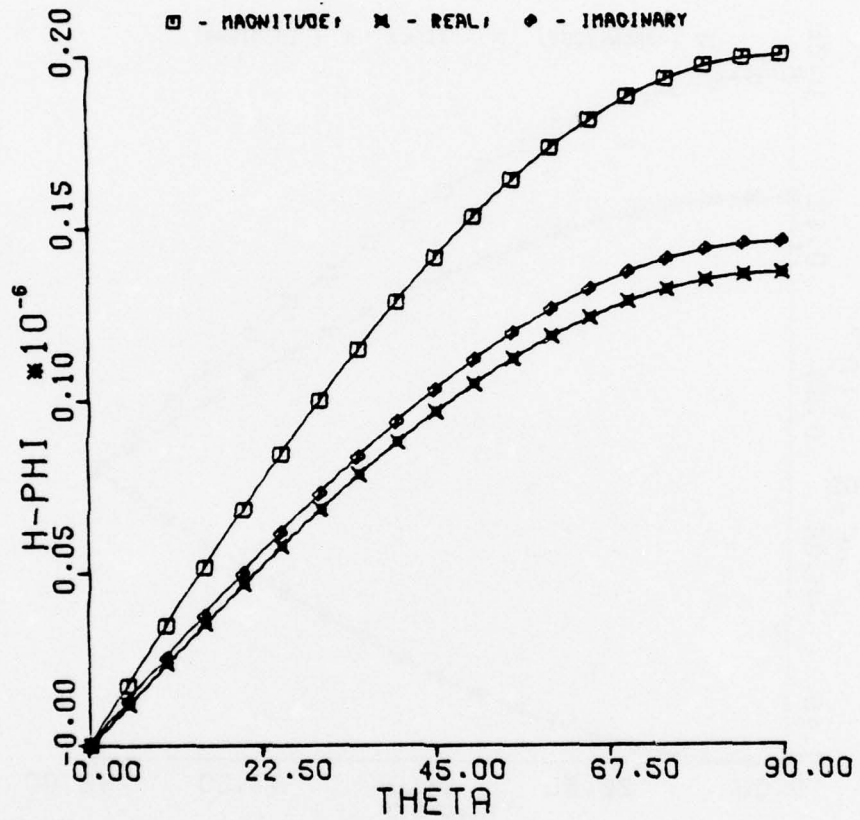


Figure 26. H_{ϕ} radiation pattern for unloaded cone with topcap, $L=54.05\text{m}$, $\theta_0 = 42.26^\circ$, $V_0 = 1$ Volt, $f = 550$ KHz, $r = 10^4\text{m}$.

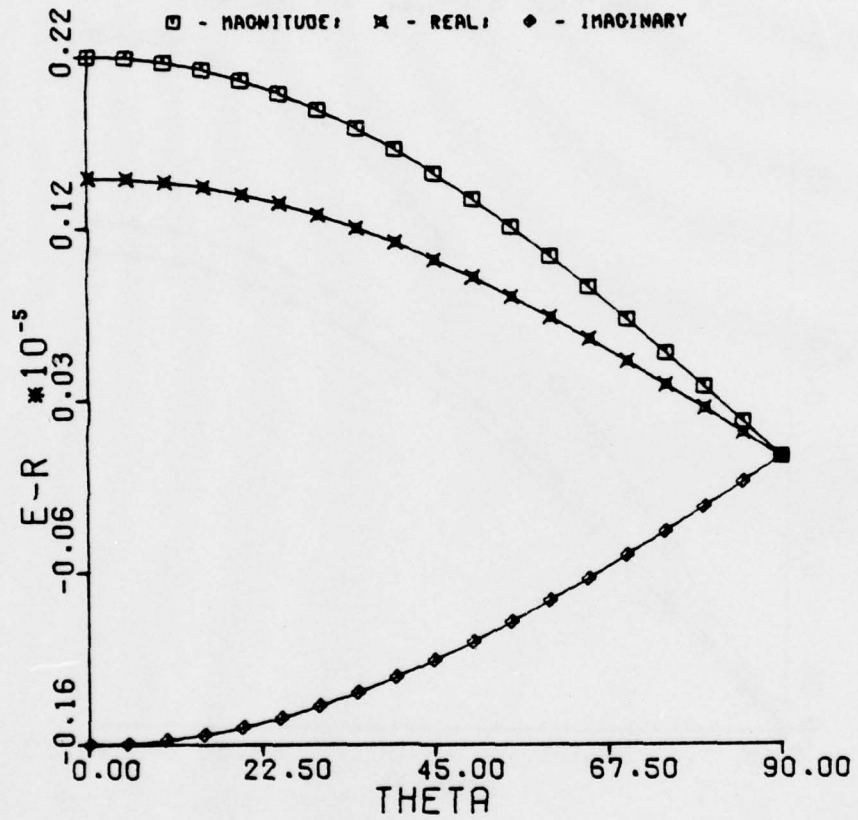


Figure 27. E_r radiation pattern for unloaded cone with topcap, $L=54.05\text{m}$, $\theta = 42.26^\circ$, $V_0 = 1 \text{ Volt}$, $f = 550 \text{ KHz}$, $r = 10^4\text{m}$.

would be a logical extension of the present problem. To be done efficiently, however, some improvements in the present computer code should be implemented. Specifically, an adaptive integration procedure should be employed to handle the integrations over the conical current subdomains, whose radii vary drastically from regions near the feed to those near the cone edge. The present code uses a fixed order quadrature rule for all segments on the structure. Additional parameter studies can be carried out using the present code to assess the effects of lumped vs. distributed loading and the effects of various load distributions on the performance of the simulator. A more ambitious project would more carefully model the actual wire structure with loading.

One conclusion of this and the companion study [1] is that the addition of a topcap does not significantly change the electromagnetic parameters of the structure - at low frequencies, the static capacitance and effective heights are almost unchanged and at the higher frequencies, the loading and the sharp angle at the edge tend to prevent current from flowing on the topcap. This observation may have some impact on the design of future simulators.

ACKNOWLEDGEMENT

The author gratefully acknowledges the able assistance of Mr. Allen Glisson in carrying out the computations.

REFERENCES

1. D.R. Wilton, "Static Analysis of Conical Antenna over a Ground Plane," Final Report, Grant No. AFOSR 75-2832, Air Force Office of Scientific Research, Bolling Air Force Base, Washington, D.C., August, 1976.
2. R.F. Harrington, Time-Harmonic Electromagnetic Fields, McGraw-Hill, New York, 1961.
3. F.M. Tesche, A.R. Neureuther, and R.E. Stovall, "The Analysis of Monopole Antennas Located on a Spherical Vehicle," Interaction Note 198, Air Force Weapons Laboratory, Albuquerque, New Mexico, October, 1974.
4. R.F. Harrington, Field Computation by Moment Methods Macmillan, New York, 1968.
5. S.A. Schelkunoff, Electromagnetic Waves, Van Nostrand, Princeton, 1943.
6. W.S. Kehrer and C.E. Baum, "Electromagnetic Design Parameters for ATHAMAS II," ATHAMAS Memos, Memo No. 4, Air Force Weapons Laboratory, Albuquerque, New Mexico, May, 1975.
7. D.S. Jones, The Theory of Electromagnetism, Pergamon, London, 1964.

APPENDIX A
CALCULATION OF RADIATED FIELDS

Once numerical values for the current distribution have been determined, the fields radiated by the bicone structure can readily be determined. Because of the symmetry of the structure and the excitation, the only non-zero components of the electric and magnetic fields are E_r , E_θ , and H_ϕ . These are defined in terms of the vector and scalar potentials as

$$\begin{aligned}
 E_r &= -j\omega A_r - \frac{\partial \phi}{\partial r} \\
 E_\theta &= -j\omega A_\theta - \frac{1}{r} \frac{\partial \phi}{\partial \theta} \\
 \mu H_\phi &= \frac{1}{r} A_\theta + \frac{\partial A_\theta}{\partial r} - \frac{1}{r} \frac{\partial A_r}{\partial \theta} \quad (A-1)
 \end{aligned}$$

where $\bar{A} = A_r \hat{r} + A_\theta \hat{\theta}$. A spherical coordinate system centered at the bicone feed and with θ measured from the z-axis is assumed. Since the fields are ϕ -independent, all fields are evaluated in the x-z plane where $\phi = 0$. The vector potential and scalar potential are given by

$$\begin{aligned}
 A_p(r, \theta) &= \frac{\mu}{8\pi^2} \left\{ \frac{I_1}{2} \psi_{pc}(r, \theta, r_1 + \Delta r_c/4) \right. \\
 &\quad \left. + \sum_{n=2}^{N_c} I_n \psi_{pc}(r, \theta, r_n) + \right.
 \end{aligned}$$

$$\begin{aligned}
& + \frac{I_{N_c+1}}{2} \left[\Psi_{pc} \left(r, \theta, L - \frac{\Delta r_c}{4} \right) + \Psi_{pt} \left(r, \theta, r_{N_c+1} - \frac{\Delta r_t}{4} \right) \right] \\
& + \left. \sum_{n=N_c+2}^N I_n \Psi_{pt} (r, \theta, r_n) \right\}; p = r, \theta \quad (A-2)
\end{aligned}$$

$$\begin{aligned}
\Phi(r, \theta) = & \frac{-1}{8\pi^2 j\omega\epsilon} \left[\sum_{n=1}^{N_c} \left(\frac{I_{n+1} - I_n}{\Delta r_c} \right) \psi_c \left(r, \theta, r_n + \frac{\Delta r_c}{2} \right) \right. \\
& \left. + \sum_{n=N_c+1}^N \left(\frac{I_{n+1} - I_n}{\Delta r_t} \right) \psi_t \left(r, \theta, r_n - \frac{\Delta r_t}{2} \right) \right] \quad (A-3)
\end{aligned}$$

where the currents and coordinates are defined in Section IV.

The potential functions Ψ and ψ are defined as

$$\Psi_{pq}(r, \theta, r_q) = \Delta r_q \int_0^{2\pi} \left(\cos \xi_{pq}^+ \frac{e^{-jkR_q^+}}{R_q^+} + \cos \xi_{pq}^- \frac{e^{-jkR_q^-}}{R_q^-} \right) d\phi' \quad (A-4)$$

$$\psi_q(r, \theta, r_q) = \Delta r_q \int_0^{2\pi} \left(\frac{e^{-jkR_q^+}}{R_q^+} - \frac{e^{-jkR_q^-}}{R_q^-} \right) d\phi', \quad p=r, \theta; q=c, t \quad (A-5)$$

where

$$\cos \xi_{rc}^{\pm} = \pm \sin \theta \cos \phi' \sin \theta_0 + \cos \theta \cos \theta_0$$

$$\cos \xi_{\theta c}^{\pm} = \pm \cos \theta \cos \phi' \sin \theta_0 - \sin \theta \cos \theta_0$$

$$\cos \xi_{rt}^{\pm} = \mp \sin \theta \cos \phi'$$

$$\cos \xi_{\theta t}^{\pm} = \mp \cos \theta \cos \phi'$$

and the radius vectors are all of the form

$$R_q^{\pm} = \sqrt{r_q'^2 + 2b_q^{\pm} r_q' + c_q^{\pm}}$$

with

$$b_c^\pm = -r \cos \phi' \sin \theta \sin \theta_0 \mp r \cos \theta \cos \theta_0 - a \cot \theta_0$$

$$c_c^\pm = r^2 \pm 2ra \cos \theta \csc \theta_0 + a^2 \csc^2 \theta_0$$

$$b_t^\pm = -r \sin \theta \cos \phi'$$

$$c_c^\pm = r^2 \mp 2rL \cos \theta \cos \theta_0 + L^2$$

Assuming a suitable choice for Δr and $\Delta \theta$, one may approximately compute the fields in (A-1) by finite difference approximations;

$$E_r(r, \theta) = -j\omega A_r(r, \theta) - \frac{\Phi(r+\Delta r, \theta) - \Phi(r, \theta)}{\Delta r}$$

$$E_\theta(r, \theta) = -j\omega A_\theta(r, \theta) - \frac{\Phi(r, \theta+\Delta \theta) - \Phi(r, \theta)}{r\Delta \theta}$$

$$\mu H_\phi = \frac{1}{r} A_\theta(r, \theta) + \frac{A_\theta(r+\Delta r, \theta) - A_\theta(r, \theta)}{\Delta r}$$

$$- \frac{A_r(r, \theta+\Delta \theta) - A_r(r, \theta)}{r\Delta \theta}$$

(A-6)

APPENDIX B
AN ALTERNATE INTEGRAL EQUATION FOR
A CONE WITH TOPCAP

The purpose of this appendix is to show how a novel identity involving the free space Green's function may be used to change the integral equation into a form where the testing procedure of Section III is applicable. In exchange for simplicity in the form resulting from the testing procedure, however, one obtains extremely complicated kernels in the integral equation. Furthermore, the new kernels have a number of singularities other than the usual one where match points and field points coincide. These complications make both the analysis and the numerical treatment tedious. Nevertheless, numerical results have been obtained for several cases using the approach and the results are in good agreement with data obtained by the method of Section III. For simplicity, we treat here only the unloaded cone.

As a prelude to the integral equation derivation, we derive a transformation of the formula for electric field components. Consider the x-component of electric field given by

$$\begin{aligned} j\omega\mu\epsilon E_x &= \hat{x} \cdot (k^2 + \nabla\nabla \cdot) \bar{A} \\ &= k^2 A_x + \frac{\partial}{\partial x} (\nabla \cdot \bar{A}) \\ &= \left(\frac{\partial^2}{\partial x^2} + k^2 \right) A_x + \frac{\partial^2 A_y}{\partial x \partial y} + \frac{\partial^2 A_z}{\partial x \partial z} \end{aligned} \quad (B-1)$$

where the vector potential \bar{A} in terms of current density \bar{J} is

$$\bar{A} = \frac{\mu}{4\pi} \int_V \bar{J} \frac{e^{-jk|\bar{r}-\bar{r}'|}}{|\bar{r}-\bar{r}'|} dV' \quad (B-2)$$

The identity

$$\frac{\partial^2}{\partial u \partial v} \left(\frac{e^{-jkR}}{R} \right) = - \left(\frac{\partial^2}{\partial u^2} + k^2 \right) \left[\frac{uv}{v^2+w^2} \left(\frac{e^{-jkR}}{R} \right) \right] \quad (B-3)$$

where $R = \sqrt{u^2+v^2+w^2}$ can be used with $u = x-x'$, $v = y-y'$, and $w = z-z'$ to rewrite (B-1) as

$$\begin{aligned} j\omega\mu \epsilon E_x &= \left(\frac{\partial^2}{\partial x^2} + k^2 \right) \int_V \left(J_x - J_y \frac{(x-x')(y-y')}{(y-y')^2+(z-z')^2} \right. \\ &\quad \left. - J_z \frac{(x-x')(z-z')}{(y-y')^2+(z-z')^2} \right) \frac{e^{-jkR}}{R} dV' \\ &= \left(\frac{\partial^2}{\partial x^2} + k^2 \right) \int_V \left(\bar{J} \cdot \hat{x} - \frac{(x-x')[\hat{y}(y-y')+\hat{z}(z-z')]}{(y-y')^2+(z-z')^2} \right) \\ &\quad \times \frac{e^{-jkR}}{R} dV' \quad (B-4) \end{aligned}$$

The vector $\bar{r}-\bar{r}' = (x-x')\hat{x} + (y-y')\hat{y} + (z-z')\hat{z}$ can be written as the sum

$$\bar{r}-\bar{r}' = (r-r')_x \hat{x} + (r-r')_t \hat{t}$$

where

$$(\bar{r}-\bar{r}')_x = \hat{x} \cdot (\bar{r}-\bar{r}') = x-x'$$

is just the component of $\bar{r}-\bar{r}'$ along the direction of \hat{x} and

$$(\bar{r}-\bar{r}')_t \hat{t} = \bar{r}-\bar{r}' - (\bar{r}-\bar{r}')_x \hat{x}$$

is just the component of $\bar{r}-\bar{r}'$ transverse to \hat{x} . Thus,

(B-4) can be written as

$$j\omega\mu\epsilon E_x = \left(\frac{\partial^2}{\partial x^2} + k^2 \right) \int_V \bar{J} \cdot \left(\hat{x} - \frac{\hat{t}(\bar{r}-\bar{r}')_t (\bar{r}-\bar{r}')_x}{(\bar{r}-\bar{r}')_t^2} \right) \frac{e^{-jkR}}{R} dV'$$

(B-5)

Since the choice of the coordinate system is arbitrary, we may choose the x-axis parallel to some constant unit vector \hat{a} and write the component of electric field in the direction of \hat{a} to be

$$\begin{aligned} j\omega\mu\epsilon E_a &= \left(\frac{\partial^2}{\partial s^2} + k^2 \right) \int_V \bar{J} \cdot \left(\hat{a} - \frac{\hat{t}(\bar{r}-\bar{r}')_t (\bar{r}-\bar{r}')_a}{(\bar{r}-\bar{r}')_t^2} \right) \\ &\quad \times \frac{e^{-jkR}}{R} dV' \\ &= \left(\frac{\partial^2}{\partial s^2} + k^2 \right) \int_V \bar{J} \cdot \left[\hat{a} - \hat{t} \cot(\hat{a}, \bar{r}-\bar{r}') \right] \frac{e^{-jkR}}{R} dV' \end{aligned}$$

(B-6)

where now \hat{t} denotes the direction of the component of $(\bar{r}-\bar{r}')$ transverse to \hat{a} and s denotes distance along a line in the direction of \hat{a} . Note that the integrand in (B-6) is singular not only when $R=0$, but also when the angle between \hat{a} and $\bar{r}-\bar{r}'$ becomes either 0° or 180° . Since in (B-6) the

only differential operator is the harmonic operator, then along a line in the direction of \hat{a} , the testing procedure of Section III which uses piecewise sinusoids may again be used to transform the harmonic operator into a finite difference operator. This is the advantage, gained at the expense of obtaining a more complicated kernel, of employing the transformation (B-3).

Returning to the cone problem, we choose the direction of \hat{a} to be along the cone generator formed by the intersection of the $\phi=0$ plane and the cone surface, and apply the boundary conditions. After some straightforward but tedious vector projection operations, one arrives at the integral equations

$$\frac{1}{j\omega\mu\epsilon} \left(\frac{\partial^2}{\partial r_c^2} + k^2 \right) \left(\Psi_{cc} + \Psi_{ct} \right) = -V_0 \delta(r_c - 0^+),$$

$$0 \leq r_c \leq L \quad (B-7)$$

$$\frac{1}{j\omega\mu\epsilon} \left(\frac{\partial^2}{\partial r_t^2} + k^2 \right) \left(\Psi_{tc} + \Psi_{tt} \right) = 0, \quad 0 \leq r_t \leq L \sin \theta_0 \quad (B-8)$$

where

$$\Psi_{pc}(r_p) = \frac{\mu}{8\pi^2} \int_0^{2\pi} \int_0^L I_c(r'_c) (K_{pc}^+ + K_{pc}^-) dr'_c d\phi'$$

$$\Psi_{pt}(r_p) = \frac{\mu}{8\pi^2} \int_0^{2\pi} \int_0^{L \sin \theta_0} I_t(r'_t) (K_{pt}^+ + K_{pt}^-) dr'_t d\phi',$$

$$p = c \text{ or } t \quad (B-9)$$

The kernels K_{pq}^{\pm} in (B-9) are of the form

$$K_{pq}^{\pm}(r_p, r'_q, \phi') = \left(D_{pq}^{\pm}(\phi') + \frac{C_{pq}^{\pm}(r'_q, \phi') [A_{pq}^{\pm}(\phi') r'_q + B_{pq}^{\pm}(\phi')]}{R_{pq}^{\pm 2} - C_{pq}^{\pm 2}(r'_q, \phi')} \right) \times \frac{e^{-jkR_{pq}^{\pm}}}{R_{pq}^{\pm}}$$

The distance between source points and field points, R_{pq}^{\pm} , is of the form

$$R_{pq}^{\pm} = \sqrt{r'_q{}^2 + 2b_{pq}^{\pm} r'_q + c_{pq}^{\pm}}$$

and b_{pq}^{\pm} and c_{pq}^{\pm} are as defined in Section IV with "a" set equal to zero. The term C_{pq}^{\pm} may be expressed as

$$C_{pq}^{\pm} = e_{pq}^{\pm} r'_q + f_{pq}^{\pm}$$

The parameters A_{pq}^{\pm} , B_{pq}^{\pm} , D_{pq}^{\pm} , and f_{pq}^{\pm} are defined in Tables (B-1)-(B-4).

Testing Equations (B-7) and (B-8) with piecewise - sinusoidal testing functions as in Section III results in the equations

$$\frac{k}{j\omega\mu\epsilon\sin k\Delta r_c} \left\{ -\cos k\Delta r_c [\Psi_{cc}(r_{c1}) + \Psi_{ct}(r_{c1})] + [\Psi_{cc}(r_{c2}) + \Psi_{ct}(r_{c2})] \right\} = -V_0 \quad (B-10)$$

TABLE B-1

DEFINITIONS OF PARAMETERS FOR THE KERNEL K_{cc}

$$A_{cc}^{\pm} = \sin^2 \theta_0 [\sin^2 \phi' + \cos^2 \theta_0 (\cos \phi' \mp 1)^2]$$

$$E_{cc}^{\pm} = 0$$

$$D_{cc}^{\pm} = -e_{cc}^{\pm} = \sin^2 \theta_0 \cos \phi' \pm \cos^2 \theta_0$$

$$f_{cc}^{\pm} = r_c$$

TABLE B-2

DEFINITIONS OF PARAMETERS FOR THE KERNEL K_{ct}

$$A_{ct}^{\pm} = \cos^2 \theta_0 \cos^2 \phi' + \sin^2 \phi'$$

$$B_{ct}^{\pm} = \mp L \cos^2 \theta_0 \sin \theta_0 \cos \phi'$$

$$D_{ct}^{\pm} = -e_{ct}^{\pm} = \sin \theta_0 \cos \phi'$$

$$f_{ct}^{\pm} = r_c \mp L \cos^2 \theta_0$$

TABLE B-3

DEFINITIONS OF PARAMETERS FOR THE KERNEL K_{tc}

$$A_{tc}^{\pm} = \sin^2 \theta_0 \sin^2 \phi' \pm \cos^2 \theta_0$$

$$B_{tc}^{\pm} = -L \cos^2 \theta_0$$

$$D_{tc}^{\pm} = -e_{tc}^{\pm} = \sin \theta_0 \cos \phi'$$

$$f_{tc}^{\pm} = r_t$$

TABLE B-4

DEFINITIONS OF PARAMETERS FOR THE KERNEL K_{tt}

$$A_{tt}^{\pm} = \sin^2 \phi'$$

$$B_{tt}^{\pm} = 0$$

$$D_{tt}^{\pm} = e_{tt}^{\pm} = \cos \phi'$$

$$f_{tt}^{\pm} = r_t$$

and

$$\begin{aligned} & \frac{k}{j\omega\mu\epsilon\text{sink}\Delta r_c} \left\{ [\Psi_{cc}(r_{c,m+1}) + \Psi_{ct}(r_{c,m+1})] \right. \\ & \quad - 2 \cos k\Delta r_c [\Psi_{cc}(r_{cm}) + \Psi_{ct}(r_{cm})] \\ & \quad \left. + [\Psi_{cc}(r_{c,m-1}) + \Psi_{ct}(r_{c,m-1})] \right\} = 0, \\ & \qquad \qquad \qquad m=2,3,\dots,N_c-1 \end{aligned} \tag{B-11}$$

Testing at the cone edge with a piecewise sinusoidal testing function which straddles both the cone and the topcap and which has its peak value at the cone edge, one obtains

$$\begin{aligned} & \frac{k}{j\omega\mu\epsilon\text{sink}\Delta r_c} \left\{ - \cos k\Delta r_c [\Psi_{cc}(r_{cNc}) + \Psi_{ct}(r_{cNc})] \right. \\ & \quad \left. + [\Psi_{cc}(r_{c,N_c-1}) + \Psi_{ct}(r_{c,N_c-1})] \right\} \\ & + \frac{k}{j\omega\mu\epsilon\text{sink}\Delta r_t} \left\{ - \cos k\Delta r_t [\Psi_{tc}(r_{t1}) + \Psi_{tt}(r_{t1})] \right. \\ & \quad \left. + [\Psi_{tc}(r_{t2}) + \Psi_{tt}(r_{t2})] \right\} \\ & + \frac{1}{j\omega\mu\epsilon} \left\{ \left[\frac{\partial \Psi_{cc}}{\partial r_c} + \frac{\partial \Psi_{ct}}{\partial r_c} \right]_{r_c=r_{cNc}} + \left[\frac{\partial \Psi_{tc}}{\partial r_t} + \frac{\partial \Psi_{tt}}{\partial r_t} \right]_{r_t=r_{t1}} \right\} = 0 \end{aligned} \tag{B-12}$$

Finally, testing on the topcap surface yields

$$\begin{aligned} & \frac{k}{j\omega\mu\epsilon\text{sink}\Delta r_t} \left\{ [\Psi_{tc}(r_{t,m+1}) + \Psi_{tt}(r_{t,m+1})] \right. \\ & \quad \left. - 2 \cos k\Delta r_t [\Psi_{tc}(r_{tm}) + \Psi_{tt}(r_{tm})] + \right. \end{aligned}$$

$$+ [\psi_{tc}(r_{t,m-1}) + \psi_{tt}(r_{t,m-1})] \} = 0, \quad m=2,3,\dots,N_t+1 \quad (B-13)$$

Substitution of the current expansions, Eqs. (40) and (41) of Section IV, into (B-10)-(B-13) yields a matrix equation for the determination of the unknown current coefficients. Because of the pulse expansion for the current, the matrix elements involve integrals like (B-9) but with the current in (B-9) equal to unity and the limits on the radial integration replaced by the limits of the corresponding current subdomain. According to (B-12), the term at the edge also requires the derivative of such integrals. In the following, we present a procedure for approximately evaluating the radial integration, leaving the ϕ' integration to be done numerically. The required integrals are all of the form

$$\int_{r_{n-}}^{r_{n+}} K dr' = \int_{r_{n-}}^{r_{n+}} \left[D + \frac{C(Ar'+B)}{R^2-C^2} \right] \frac{e^{-jkR}}{R} dr' \quad (B-14)$$

where, for convenience, all subscripts and superscripts have been suppressed. Since the number of subdomains should be chosen such that $k|r_{n+} - r_{n-}|$ is small, we chose some point r_n in the interval $[r_{n+}, r_{n-}]$ and expand $\exp(-jkR)$ in a Taylor series about the point $r' = r_n$;

$$\begin{aligned}
e^{-jkR} &= e^{-jkR_n} e^{-jk(R-R_n)} \\
&\approx e^{-jkR_n} [1 - jk(R-R_n)] \quad (B-15)
\end{aligned}$$

where R_n denotes R evaluated at $r'=r_n$. The resulting approximate integral is

$$\begin{aligned}
\int_{r_{n-}}^{r_{n+}} K dr' &\approx e^{-jkR_n} \int_{r_{n-}}^{r_{n+}} \left[D + \frac{C(Ar'+B)}{R^2-C^2} \right] \left[\frac{1-jk(R-R_n)}{R} \right] dr' \\
&= e^{-jkR_n} (I_1 + I_2 + I_3) \quad (B-16)
\end{aligned}$$

where

$$I_1 = -jk \int_{r_{n-}}^{r_{n+}} \left(D + \frac{C(Ar'+B)}{R^2-C^2} \right) dr'$$

$$I_2 = D(1+jkR_n) \int_{r_{n-}}^{r_{n+}} \frac{dr'}{R}$$

and

$$I_3 = (1+jkR_n) \int_{r_{n-}}^{r_{n+}} \frac{C(Ar'+B)}{R^2-C^2} \frac{dr'}{R}$$

The first integral may be evaluated by substituting the definitions for R and C in terms of b, c, e , and f ;

$$\begin{aligned}
I_1 &= -jk \int_{r_{n-}}^{r_{n+}} \left(D + \frac{Aer'^2 + (Be+Af)r' + Bf}{(1-e^2)r'^2 + 2(b-ef)r' + c-f^2} \right) dr' \\
&= -jk \left\{ F_1(r_{n+} - r_{n-}) + F_2 \ln \left| \frac{R_{n+}^2 - C_{n+}^2}{R_{n-}^2 - C_{n-}^2} \right| \right. \\
&\quad + F_3 \left[\tan^{-1} \left(\frac{(1-e^2)r_{n+} + (b-ef)}{\sqrt{(1-e^2)(c-f^2) - (b-ef)^2}} \right) \right. \\
&\quad \left. \left. - \tan^{-1} \left(\frac{(1-e^2)r_{n-} + (b-ef)}{\sqrt{(1-e^2)(c-f^2) - (b-ef)^2}} \right) \right] \right\} \quad (B-17)
\end{aligned}$$

where

$$F_1 = D + \frac{Ae}{1-e^2}$$

$$F_2 = \frac{(Be+Af)(1-e^2) - 2Ae(b-ef)}{2(1-e^2)^2}$$

$$\begin{aligned}
F_3 &= [2Ae(b-ef)^2 - Ae(1-e^2)(c-f^2) - (Be+Af)(b-ef)(1-e^2) + Bf(1-e^2)^2] \\
&\quad \times [(1-e^2)^2 \sqrt{(1-e^2)(c-f^2) - (b-ef)^2}]^{-1}
\end{aligned}$$

The tabulated integrals Dw 160.01, 160.11, and 160.21 aid in the evaluation of I_1 .[†] I_2 may be evaluated using Dw. 380.001

as

$$I_2 = D(1+jkR_n) \int_{r_{n-}}^{r_{n+}} \frac{dr'}{R}$$

[†]The abbreviations Dw and GR refer to Tables of Integrals and other Mathematical Data, Fourth Ed., H.B. Dwight, Macmillan, N.Y., 1961; and Tables of Integrals, Series and Products, I.S. Gradshteyn and I.W. Ryshik, Academic Press, N.Y., 1965, respectively.

$$= D(1+jkR_n) \ln \frac{R_{n+} + r_{n+} + b}{R_{n-} + r_{n-} + b} \quad (B-18)$$

The subscripts n , $n+$, and $n-$ denote quantities which are evaluated at $r'=r_n$, r_{n+} , and r_{n-} , respectively.

The evaluation of I_3 is facilitated by expanding it in partial fractions and using the substitution $\sinh \theta = (r'+b)/\sqrt{c-b^2}$ to obtain

$$\begin{aligned} I_3 &= (1+jkR_n) \int_{r_{n-}}^{r_{n+}} \frac{C(Ar'+B)}{R^2-C^2} dr' \\ &= \frac{(1+jkR_n)}{2} \int_{r_{n-}}^{r_{n+}} \left(\frac{1}{R-C} - \frac{1}{R+C} \right) \frac{(Ar'+B)}{R} dr' \\ &= \frac{(1+jkR_n)}{2} \int_{\theta_{n-}}^{\theta_{n+}} (A\sqrt{c-b^2} \sinh \theta + B-Ab) \\ &\quad \times \left(\frac{1}{\sqrt{c-b^2} \cosh \theta - e^{\sqrt{c-b^2} \sinh \theta} - f+be} \right. \\ &\quad \left. - \frac{1}{\sqrt{c-b^2} \cosh \theta + e^{\sqrt{c-b^2} \sinh \theta} + f-be} \right) d\theta \end{aligned}$$

Using GR 2.451.2 and GR 2.451.4, one finds the latter integral to be

$$\begin{aligned}
I_3 = & (1+jkR_n) \left[\frac{Ae}{1-e^2} \ln \left| \frac{R_{n+} + r_{n+} + b}{R_{n-} + r_{n-} + b} \right| \right. \\
& + \frac{A}{2(1-e^2)} \ln \left| \frac{(R_{n+} - C_{n+})(R_{n-} + C_{n-})}{(R_{n-} - C_{n-})(R_{n+} + C_{n+})} \right| \\
& + F_4 \left[\tan^{-1} \frac{\sqrt{c-b^2}(R_{n-} - C_{n-}) - (be-f)R_{n+} + b^2 - c}{F_5(r_{n+} + b)} \right. \\
& - \tan^{-1} \frac{\sqrt{c-b^2}(R_{n-} - C_{n-}) - (be-f)R_{n-} + b^2 - c}{F_5(r_{n-} + b)} \\
& - \tan^{-1} \frac{\sqrt{c-b^2}(R_{n+} + C_{n+}) + (be-f)R_{n+} + b^2 - c}{F_5(r_{n+} + b)} \\
& \left. \left. + \tan^{-1} \frac{\sqrt{c-b^2}(R_{n-} + C_{n-}) + (be-f)R_{n-} + b^2 - c}{F_5(r_{n-} + b)} \right] \right] \quad (B-19)
\end{aligned}$$

where

$$F_4 = \frac{(B-Ab)(1-e^2) - Ae(be-f)}{F_5(1-e^2)}$$

$$F_5 = \sqrt{(c-b^2(1-e^2) - (be-f)^2)}$$

Equations (B-17)-(B-19) complete the evaluation of (B-16).

The derivative terms appearing in (B-12) require evaluation of integrals of the form

$$\frac{\partial}{\partial r} \int_{r_{n-}}^{r_{n+}} K dr' = \frac{\partial}{\partial r} \int_{r_{n-}}^{r_{n+}} \left[D + \frac{C(Ar'^4 + B)}{R^2 - C^2} \right] \frac{e^{-jkR}}{R} dr' \quad (B-20)$$

where the unprimed variable r is r_c or r_t , as appropriate. The two edge terms also have non-integrable singularities at the edge which cancel between the various terms. To handle this situation numerically, the singularity must be explicitly identified and removed for numerical integration. Thus the same kind of approximate analytical integration of (B-20) as used to evaluate (B-16) would both eliminate one integration and explicitly identify the singular term. The derivative can be taken inside the integral if care is taken to identify the singular terms. Noting that $\partial C/\partial r = 1$, $\partial (R^2 - C^2)/\partial r = 0$, and $\partial A/\partial r = \partial B/\partial r = 0$, we have

$$\frac{\partial}{\partial r} \int_{r_{n-}}^{r_{n+}} K dr' = \int_{r_{n-}}^{r_{n+}} \left[-\frac{jkDC}{R^2} - \frac{DC}{R^3} + \frac{Ar'+B}{R^2-C^2} \left(\frac{1}{R} - \frac{jkC^2}{R^2} - \frac{C^2}{R^3} \right) \right] e^{-jkR} dr'$$

With the approximation of (B-15), the above may be written as

$$\int_{r_{n-}}^{r_{n+}} \frac{\partial K}{\partial r} dr' \approx e^{-jkR_n} (I_4 + I_3 + I_6 + I_7 + I_8) \quad (B-21)$$

The various integrals appearing in (B-21) are defined and evaluated as follows:

$$\begin{aligned}
I_4 &= -k^2 \int_{r_{n-}}^{r_{n+}} \frac{CD}{R} dr' = -k^2 \int_{r_{n-}}^{r_{n+}} \frac{D(er'+f)}{R} dr' \\
&= -k^2 \left[De(R_{n+} - R_{n-}) - (be-f) \ln \left| \frac{R_{n+} + r_{n+} + b}{R_{n-} + r_{n-} + b} \right| \right] \quad (B-22)
\end{aligned}$$

where Dw 380.001 and Dw 380.011 have been used.

$$\begin{aligned}
I_5 &= k^2 R_n \int_{r_{n-}}^{r_{n+}} \frac{(De-A)r' + fD - B}{r'^2 + 2br' + c} dr' \\
&= k^2 R_n \left[(De-A) \ln \left| \frac{R_{n+}}{R_{n-}} \right| \right. \\
&\quad \left. + \frac{fD - B - b(De-A)}{\sqrt{c-b^2}} \left(\tan^{-1} \frac{r_{n+} + b}{\sqrt{c-b^2}} - \tan^{-1} \frac{r_{n-} + b}{\sqrt{c-b^2}} \right) \right] \quad (E-23)
\end{aligned}$$

where Dw 160.01 and Dw 160.11 have been used. Using Dw 300.003 and Dw 380.013, one obtains

$$\begin{aligned}
I_6 &= (1+jkR_n) \int_{r_{n-}}^{r_{n+}} \frac{(A-De)r' + (B-Df)}{R^3} dr' \\
&= \frac{1+jkR_n}{c-b^2} \left\{ [B-Df - b(A-De)] \left(\frac{r_{n+}}{R_{n+}} - \frac{r_{n-}}{R_{n-}} \right) \right. \\
&\quad \left. + [b(B-Df) - c(A-De)] \left(\frac{1}{R_{n+}} - \frac{1}{R_{n-}} \right) \right\} \quad (B-24)
\end{aligned}$$

Again using Dw 160.01 and Dw 160.11, we have

$$\begin{aligned}
 I_7 &= -jk(1+jkR_n) \int_{r_{n-}}^{r_{n+}} \frac{Ar'+B}{R^2-C^2} dr' \\
 &= -jk(1+jkR_n) \int_{r_{n-}}^{r_{n+}} \frac{Ar'+B}{(1-e^2)r'^2+2(b-ef)r'+c-f^2} dr' \\
 &= -jk(1+jkR_n) \left\{ \frac{A}{2(1-e^2)} \ln \left| \frac{R_{n+}^2-C_{n+}^2}{R_{n-}^2-C_{n-}^2} \right| \right. \\
 &\quad \left. + \frac{B(1-e^2)-(b-ef)A}{(1-e^2)F_6} \left[\tan^{-1} \left(\frac{(1-e^2)r_{n+}+b-ef}{F_6} \right) \right. \right. \\
 &\quad \left. \left. - \tan^{-1} \left(\frac{(1-e^2)r_{n-}+b-ef}{F_6} \right) \right] \right\}
 \end{aligned}$$

(B-25)

where

$$F_6 = \sqrt{(1-e^2)(c-f^2)-(b-ef)^2}$$

The remaining integral is

$$\begin{aligned}
 I_8 &= k^2 \int_{r_{n-}}^{r_{n+}} (Ar'+B) \left(\frac{1}{R} - \frac{R}{R^2-C^2} \right) dr' \\
 &= -k^2 \int_{r_{n-}}^{r_{n+}} \frac{C^2(Ar'+B)}{R(R^2-C^2)} dr'
 \end{aligned}$$

$$= -k^2 \int_{r_{n-}}^{r_{n+}} \frac{C(er'+f)(Ar'+B)}{R(R^2-C^2)} dr'$$

$$= -k^2 \int_{r_{n-}}^{r_{n+}} \frac{C[Aer'^2+(Af+Be)r'+Bf]}{R(R^2-C^2)} dr'$$

Dividing $R^2-C^2 = (1-e^2)r'^2 + 2(b-ef)r'+c-f^2$ into the bracketed term in the numerator of the integrand, we may write the integral as

$$I_8 = -k^2 \int_{r_{n-}}^{r_{n+}} \frac{C}{R} \left[\frac{Ae}{1-e^2} + \frac{(Af+Be+W)r'+Bf+U}{R^2-C^2} \right] dr'$$

where

$$W = - \frac{2Ae(b-ef)}{1-e^2}$$

$$U = - \frac{Ae(c-f^2)}{1-e^2}$$

Expanding the second term in brackets in the integrand in partial fractions, one can write I_8 as

$$I_8 = I_8' + I_8''$$

where

$$I_8' = \frac{-k^2 Ae}{1-e^2} \int_{r_{n-}}^{r_{n+}} \frac{er'+f}{R} dr'$$

$$= \frac{-k^2 Ae}{1-e^2} \left[e(R_{n+}-R_{n-}) + (f-be) \ln \left| \frac{R_{n+}+r_{n+}+b}{R_{n-}+r_{n-}+b} \right| \right]$$

and

$$I_8'' = \frac{-k^2}{2} \int_{r_{n-}}^{r_{n+}} [(Af+Be+W)r'+Bf+U] \left(\frac{1}{R-C} - \frac{1}{R+C} \right) \frac{dr'}{R}$$

The substitution $\sinh \theta = (r'+b)/\sqrt{c-b^2}$ enables one to write

I_8'' as

$$I_8'' = \frac{-k^2}{2} \int_{\theta_{n-}}^{\theta_{n+}} [(Af+Be+W)\sqrt{c-b^2} \sinh \theta + Bf+U-b(Af+Be+W)] \\ \times \left(\frac{1}{\sqrt{c-b^2} \cosh \theta - e\sqrt{c-b^2} \sinh \theta - f+be} - \frac{1}{\sqrt{c-b^2} \cosh \theta + e\sqrt{c-b^2} \sinh \theta + f-be} \right) d\theta$$

Using GR 2.451.2 and GR 2.451.4, we obtain finally

$$I_8'' = -k^2 \left\{ \frac{Af+Be+W}{2(1-e^2)} \ln \left| \frac{(R_{n+}-C_{n+})(R_{n-}+C_{n-})}{(R_{n-}-C_{n-})(R_{n+}+C_{n+})} \right| \right. \\ \left. + \frac{e(Af+Be+W)}{(1-e^2)} \ln \left| \frac{R_{n+}+r_{n+}+b}{R_{n-}+r_{n-}+b} \right| \right. \\ \left. + F_7 \left[\tan^{-1} \left(\frac{\sqrt{c-b^2}(R_{n+}-C_{n+})-(be-f)R_{n+}+b^2-c}{(r_{n+}+b)F_5} \right) \right. \right. \\ \left. \left. - \tan^{-1} \left(\frac{\sqrt{c-b^2}(R_{n-}-C_{n-})-(be-f)R_{n-}+b^2-c}{(r_{n-}+b)F_5} \right) \right] \right\}$$

$$\begin{aligned}
& - \tan^{-1} \left\{ \frac{\sqrt{c-b^2}(R_{n+}+C_{n+}) + (be-f)R_{n+}+b^2-c}{(r_{n+}+b)F_5} \right\} \\
& + \tan^{-1} \left\{ \frac{\sqrt{c-b^2}(R_{n-}+C_{n-}) + (be-f)R_{n-}+b^2-c}{(r_{n-}+b)F_5} \right\} \Bigg\} \quad (B-27)
\end{aligned}$$

where

$$F_7 = \frac{[Bf+U-b(Af+Be+W)](1-e^2)-e(be-f)(Af+Be+W)}{(1-e^2)F_5}$$

Equations (B-22) through (B-27) complete the evaluation of the integral, (B-21). Recall that the integral (B-21) needs to be evaluated only for observation points at the bicone edge (see Eq. (B-12)). For the source current pulse associated with the bicone edge, there results a non-integrable singularity (with respect to ϕ' integration) which comes from the term $1/R_{n+}$ in (B-24). Each of the derivative terms in (B-12) contains such a non-integrable singularity, however, and they are of opposite signs so as to cancel each other. For numerical integration, of course, the canceling singularities must be analytically subtracted.

The integrals I_1 through I_8 contain integrable singularities such as the usual one where source and field points coincide (i.e., $R=0$). In addition, however, there are also integrable singularities introduced by the transformation (B-6). These arise from current sources which lie along and are directed transverse to the line which passes through the observation point and which is in the direction of the

electric field component of interest. For example, in computing the tangential field component E_{r_c} on the cone, singularities arise from currents on the topcap and its image. While the many singularities complicate the numerical procedure, they can, in principle, be handled. However, the unwieldiness of the functions appearing in the integrals I_1 through I_8 makes the numerical procedure rather inefficient and subject to error. For example, the computer code derived from the formulation presented here seemed to yield reasonable results for moderate cone angles, but often yielded erroneous results for the very small cone angles used to check the program. The complexity of the formulation became a considerable hinderance in determining the source of these difficulties. Consequently, the final calculations were done using the formulation of Section III which was developed as an extension of methods currently being used to treat flat plate surfaces.